Hochschule
München (HM)
University of
Applied Sciences

Laboratory for
Mechatronic
and Renewable
Energy Systems
(LMRES)

Frequency-adaptive pole placement for parallelized proportional, integral and resonant control systems

Christoph Göttsberger and Christoph M. Hackl
christoph.hackl@hm.edu

2026.01.08, Universidad Técnica Federico Santa María, Valparaiso, Chile

HM

ISES

Outline

Introduction

Research environment: HM (www.hm.edu), ISES (ises.hm.edu) and LMRES (lmres.ee.hm.edu)

HM ISES LMRES

HM – Munich University of Applied Sciences

- 14 departmens
- >18.000 students
- ~480 professors
- 3 campuses

ISES – Institute for Sustainable Energy Systems

- 8 research labs (8 professors)
- 45 PhD candidates

LMRES – Laboratory for Mechatronic and Renewable Energy Systems

- International team
- 15 PhD candidates
- >150 publications / >10.7 Mio. € raised

Introduction

LMRES – Research projects and research goals (funding: > 9.2 million €; e.g. DAAD, Bavaria, BMBF, BMWi, DFG, EU)

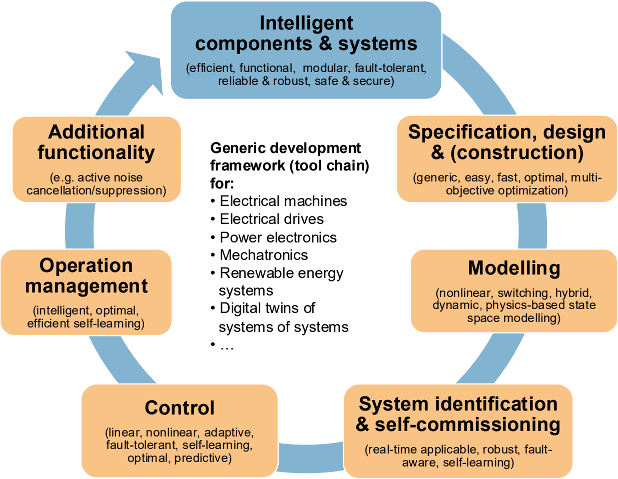

Introduction

LMRES – Interdisciplinary expertise & selected publications (> 150 peer-reviewed contributions)

System identification [9–26]

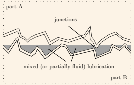

Friction [27–29]

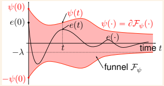

Non-identifier based adaptive control [14, 27, 30–46]

Paper coating machines [4–8]

Supervision & teaching (Award) [159–165]

Mechatronics & robotics [27, 28, 40, 46–58]

Mechatronic and renewable energy systems

Electro-active polymers [1–3]

Power electronics [19–21, 46, 58–88]

Wind energy, renewables & smart grid [13–15, 44, 46, 57, 58, 60, 61, 67, 68, 70–72, 74, 79, 85, 93–95, 98, 100, 107, 112, 120, 132, 136, 141–158]

Electrical machines & drives [13, 15, 17, 23–27, 30, 32, 33, 45, 46, 51, 55, 57, 69, 77, 78, 80, 89–140]

Introduction

LMRES – Selected research results: Smart grid/renewables/power systems (multi-level converters; fault-tolerance) [166]

IES Industrial Electronics Society

Received 24 January 2025; revised 26 March 2025; accepted 10 April 2025. Date of publication 14 April 2025; date of current version 12 May 2025. The review of this article was arranged by Associate Editor Binbin Li.

Digital Object Identifier 10.1109/OJIES.2025.3560741

Cluster-Fault Control Strategies for Modular Multilevel Converters

OLIVER KALMBACH (Graduate Student Member, IEEE) AND CHRISTOPH M. HACKL (Senior Member, IEEE)

Laboratory for Mechatronic and Renewable Energy Systems, Hochschule München University of Applied Sciences, 80335 Munich, Germany

CORRESPONDING AUTHOR: CHRISTOPH M. HACKL (e-mail: christoph.hackl@hm.edu).

This work was supported in part by the Munich University of Applied Sciences HM and in part by the Deutsche Forschungsgemeinschaft (DFG, German Research Foundation) - Project under Grant 512819356.

ABSTRACT Modular multilevel converters (MMCs) are widely used for high-voltage and high-power applications. They are highly scalable, modular, and flexible in operation. However, this comes with the price of a large number of components, such as semiconductors and capacitors. Each of those components is prone to failure. This article presents four fault-tolerant control strategies for MMCs under severe failures: cluster faults that have been rarely discussed in literature for MMCs. Three fault modes are discussed and four cluster-fault control strategies are proposed. All approaches are derived in detail and validated by simulation and measurement results, including transitions from healthy to faulty operation for different power factors and power steps. The results show that proper functionality of the MMC by the proposed cluster-fault control strategies is still achievable even under the resulting voltage constraints. The proposed cluster-fault control strategies are simple to implement and allow for 1) an easy integration into (existing) systems and 2) an improved fault tolerance of MMCs.

INDEX TERMS Cluster fault, cluster-fault operation, cluster-fault control, fault tolerance, fault-tolerant control, high-voltage direct current (HVDC), input/output (I/O) linearization, modular multilevel cascade converter (MMCC), modular multilevel converter (MMC).

I. INTRODUCTION

In 2001, the modular multilevel cascade converter (MMCC) [1] was introduced by Marquardt et al. [2], [3]. Since then, hundreds of researchers have focused on series-connected (cascaded) cells. Usually, chopper cells (CCs) are used due to their simplicity and costs (MMCC-DSCC). However, for certain topologies, bridge cells (BCs), leading to MMCC-DSBC, are better suited, for example, if a

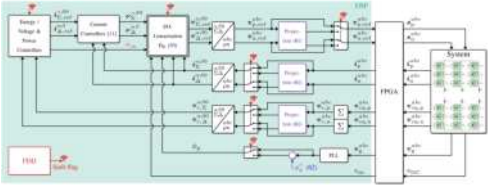

FIGURE 2. Cluster-fault-tolerant control structure. The essential components are the fault-tolerant cluster voltage/energy control and the I/O linearization current control. Both are adjusted in case an FDD block triggers a fault. In addition, the projection and phase adaption blocks are highlighted, which allows for handling a cluster fault in an arbitrary cluster.

modulation index (+; see m_{S1} in Fig. 3), moderate capacitor energy fluctuations (0; see Fig. 4), and increased current stress (−; see Fig 5). Moreover, S1 does not alter the ac and dc terminal quantities (+), i.e., the faulty MMC behaves at its terminals as there was no fault.

2) STRATEGY S2

For strategy S2, ac component $v_{\rm on,ac}$, dc components $i^\beta_{\Sigma,\rm dc}$ and $i^0_{\Sigma,\rm dc}$, and, in contrast to S1, negative- and positive-sequence current amplitudes $\hat{\imath}^{d-}_\Sigma$ and $\hat{\imath}^{q+}_\Sigma$ are used as control variables. This gives

$$i^\beta_\Sigma = i^\beta_{\Sigma,\rm dc} + \hat{\imath}^{d-}_\Sigma \cos(\phi_g) - \hat{\imath}^{q+}_\Sigma \sin(\phi_g) \quad (29)$$

$$i^0_\Sigma = i^0_{\Sigma,\rm dc} - \hat{\imath}^{d-}_\Sigma \sin(\phi_g) + \hat{\imath}^{q+}_\Sigma \cos(\phi_g) \quad (30)$$

allowing for the independent mean active power control with

$$\left.\begin{aligned}
\overline{p}^\alpha_\Sigma &:= -\tfrac{1}{2} v_{\rm on,ac} i^\alpha_\Delta - \tfrac{1}{2} v_{\rm dc} i^0_{\Sigma,\rm dc} \\
\overline{p}^\beta_\Sigma &:= \tfrac{1}{2} v_{\rm dc} i^\beta_{\Sigma,\rm dc} - \tfrac{1}{2} v_{\rm on,ac} i^\beta_\Delta \\
\overline{p}^0_\Sigma &:= \tfrac{1}{2} v_{\rm dc} i^0_{\Sigma,\rm dc} \\
\overline{p}^\beta_\Delta &:= (v^\alpha_o - 2 v_{\rm on,ac}) \left(\hat{\imath}^{d-}_\Sigma \cos(\phi_g) - \hat{\imath}^{q+}_\Sigma \sin(\phi_g)\right) \\
&\quad + v^\beta_o \left(-\hat{\imath}^{d-}_\Sigma \sin(\phi_g) + \hat{\imath}^{q+}_\Sigma \cos(\phi_g)\right) \\
\overline{p}^0_\Delta &:= -v^\beta_o \left(\hat{\imath}^{d-}_\Sigma \cos(\phi_g) - \hat{\imath}^{q+}_\Sigma \sin(\phi_g)\right)
\end{aligned}\right\}.$$

S2 does slightly alter the ac and dc terminal quantities (0), as the faulty MMC will have an ac component in its dc current due to (30).

3) STRATEGY S3

The control variables for S3, as listed in Table 1, are ac components $v_{\rm on,ac}$ and $i^\beta_{\Sigma,\rm ac}$ and dc components $v_{\rm on,dc}$, $i^\beta_{\Sigma,\rm dc}$, and $i^0_{\Sigma,\rm dc}$. Hence, the common-mode voltage $v_{\rm on} = v_{\rm on,dc} + v_{\rm on,ac}$ has two components, and the regulated mean active powers for S3 become

$$\left.\begin{aligned}
\overline{p}^\alpha_\Sigma &:= -\tfrac{1}{2} v_{\rm on,ac} i^\alpha_\Delta - \tfrac{1}{2} v_{\rm dc} i^0_{\Sigma,\rm dc} \\
\overline{p}^\beta_\Sigma &:= \tfrac{1}{2} v_{\rm dc} i^\beta_{\Sigma,\rm dc} - \tfrac{1}{2} v_{\rm on,ac} i^\beta_\Delta \\
\overline{p}^0_\Sigma &:= \tfrac{1}{2} v_{\rm dc} i^0_{\Sigma,\rm dc} \\
\overline{p}^\beta_\Delta &:= (v^\alpha_o - 2 v_{\rm on,ac}) i^\beta_{\Sigma,\rm ac} - 2 v_{\rm on,dc} i^0_{\Sigma,\rm dc} \\
\overline{p}^0_\Delta &:= -v^\beta_o i^\beta_{\Sigma,\rm ac} - 2 v_{\rm on,dc} i^\beta_{\Sigma,\rm dc}
\end{aligned}\right\}. \quad (32)$$

Also, strategy S3 allows for an optional interchanging of the control variables $v_{\rm on,ac}$ and $i^\beta_{\Sigma,\rm dc}$ of $\overline{p}^\alpha_\Sigma$ and $\overline{p}^\beta_\Sigma$ and of the control variables $i^\beta_{\Sigma,\rm ac}$ and $v_{\rm on,dc}$ of $\overline{p}^\beta_\Delta$ and $\overline{p}^0_\Delta$, respectively.

Performance evaluation (pros and cons) of strategy S3: Strategy S3 exhibits the worst modulation index (−; see m_{S3} in Fig. 3), the highest capacitor energy fluctuations (−; see Fig. 4), moderate current stress (0; see Fig 5), and unchanged

Introduction

LMRES – Selected research results: Smart grid/renewables/power systems (grid-connected inverters) [167]

Received 31 January 2025; revised 24 March 2025; accepted 31 March 2025. Date of publication 3 April 2025; date of current version 30 April 2025. The review of this article was arranged by Associate Editor Marco Rivera.

Digital Object Identifier 10.1109/OJIES.2025.3557702

Modeling and Proportional-Integral State Feedback Control of Fully Parallel Grid-Connected Inverters

ZHAO SONG [1], SIMON KRÜNER [2], AND CHRISTOPH M. HACKL [1] (Senior Member, IEEE)

[1]Laboratory for Mechatronic and Renewable Energy Systems, Hochschule München University of Applied Sciences, 80335 Munich, Germany
[2]Graduate Center of Engineering and Design, Technical University of Munich, 85748 Munich, Germany

Corresponding author: CHRISTOPH M. HACKL (e-mail: christoph.hackl@hm.edu).

This work was supported by the Munich University of Applied Sciences HM and the Deutsche Forschungsgemeinschaft (DFG, German Research Foundation) under Grant 512819356.

ABSTRACT A novel three-phase grid-connected inverter topology with a split dc link and *LC* filter is proposed. It allows for a full parallel connection of multiple inverters simultaneously on both the ac and dc sides, offering high modularity, redundancy, expandability, and overall system reliability. A generic dynamical system model is derived, considering the coupling effects between parallelized inverters, physical constraints, and varying grid impedance. A decentralized proportional-integral state feedback control (PI-SFC) with an extended Luenberger state observer is developed and compared with a conventional PI controller regulating inverter-side currents. A stability analysis shows that both closed-loop control systems remain stable even if an arbitrarily large number of inverters are connected in parallel. Simulations and experiments confirm the functionality and robustness of the closed-loop system under varying grid impedances and during grid faults. For the experimental results, the controllers were implemented on commercially available hardware of the proposed topology. In particular, the PI-SFC allows for better exploitation of the full power of the inverters due to its enhanced controller performance and damping ability. Besides, the exceptional match between simulation and experimental results proves the accuracy of the proposed system model as well.

INDEX TERMS Grid-connected inverter, grid impedance, parallel inverters, split dc link, state feedback control (SFC), state space model, voltage source inverter (VSI).

NOMENCLATURE

follows. If a quantity is in bold font, it is a vector. For example,

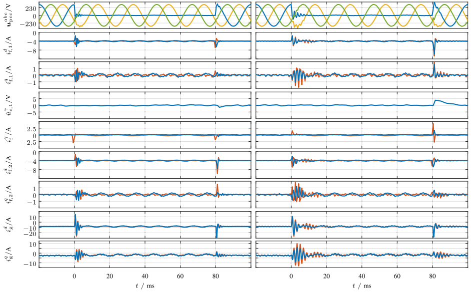

FIGURE 10. Results of Experiment II: Comparison of PI controller [—] and PI-SFC [—] under FRT conditions, with the left column showing the results with $L_g = 1$ mH and the right column with $L_g = 2$ mH.

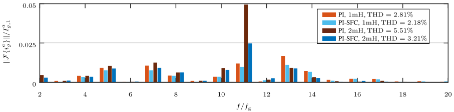

FIGURE 11. Frequency spectrum of grid current i_g^a, using the PI controller and the PI-SFC under different grid impedances, normalized to the amplitude of the fundamental frequency (identical for all cases, with $\hat{I}_{g,1}^a = 8.5$ A at $f_g = 50$ Hz).

Introduction

LMRES – Selected research results: Electrical drives (multi-objective optimization & operation, neural networks) [168]

IEEE Open Journal of the Industrial Electronics Society

Received 16 November 2023; revised 12 January 2024; accepted 17 January 2024. Date of publication 22 January 2024; date of current version 5 February 2024. The review of this paper was arranged by Associate Editor Giampaolo Buticchi.

Digital Object Identifier 10.1109/OJIES.2024.3356721

Multiobjective Hyperparameter Optimization of Artificial Neural Networks for Optimal Feedforward Torque Control of Synchronous Machines

NIKLAS MONZEN, FLORIAN STROEBL, HERBERT PALM, AND CHRISTOPH M. HACKL (Senior Member, IEEE)

Institute for Sustainable Energy Systems (ISES), Hochschule München University of Applied Sciences, 80333 Munich, Germany

CORRESPONDING AUTHOR: CHRISTOPH M. HACKL (e-mail: christoph.hackl@hm.edu).

This work was supported by the Munich University of Applied Sciences HM and the Deutsche Forschungsgemeinschaft (DFG, German Research Foundation) - Projectnumber 512819356.

ABSTRACT Multiobjective hyperparameter optimization is applied to find optimal artificial neural network (ANN) architectures used for optimal feedforward torque control (OFTC) of synchronous machines. The proposed framework allows to systematically identify Pareto optimal ANNs with respect to multiple (partly) contradictory objectives, such as approximation accuracy and computational burden of the considered ANNs. The obtained Pareto optimal ANNs are trained and implemented on a realtime system and tested experimentally for a nonlinear reluctance synchronous machine against non-Pareto optimal ANN designs and a state-of-the-art OFTC approach. Finally, based on the most recent results from ANN approximation theory, guidelines for Pareto optimal ANN-based OFTC design and implementation are provided.

INDEX TERMS Artificial neural network (ANN), hyperspace exploration (HSE), multiobjective hyperparameter optimization (MO-HPO), optimal feedforward torque control (OFTC), reluctance synchronous machine (RSM).

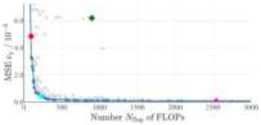

FIGURE 7. MO-HPO results of two hidden layers with the selected ANN designs: 4-4-4-2 [◆], 4-2-97-2 [◆], 4-4-14-2 [◆], 4-75-12-2 [◆].

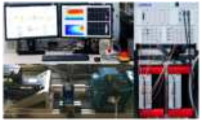

FIGURE 8. Experimental setup.

a) Scenario and Time Series: The implementation of the ANN is realized by a (self-written) MATLAB function, which is subsequently integrated into Simulink for the eventual real-time code generation. The 1.9 kW nonlinear RSM (right machine in Fig. 8) is speed controlled. The speed controller outputs the reference torque to the ANN-based OFTC system which computes the optimal reference currents for the underlying current controllers. For those, a generic and non-linear current controller structure based on I/O-linearization was applied as introduced in [47, Sec. 6.6.7] (in German) and

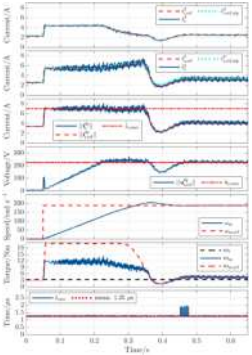

FIGURE 9. Experimental results for the proposed ANN-based OFTC (architecture 4-4-14-2) for a nonlinear RSM (from top to bottom): Time series of actual currents i_s, ANN-based OFTC reference currents $i_{s,ref}$ and NLP-based OFTC reference currents $i_{s,ref,nlp}$ (d and q), current magnitudes of actual $||i_s^{dq}||$ and reference currents $||i_{s,ref}^{dq}||$, voltage magnitude $||u_s^{dq}||$, angular velocity ω_m, torque m_m, and execution time t_{exec}.

Introduction

LMRES – Selected research results: Electrical machine design (multi-objective optimization; in preparation) [140]

1

Multi-Objective Machine Design Optimization with Gaussian Process Regression and Bayesian Optimization (Extended Version)

Johannes Rossmann, Maarten J. Kamper, *Senior Member, IEEE,*
Christoph C. Hackl, *Senior Member, IEEE*

Abstract

During the design phase of electrical machines, diverse performance specifications need to considered. Although stochastic optimization algorithms are extensively employed for this purpose, a primary drawback is the substantial number of designs requiring evaluation. Bayesian optimization presents an alternative methodology that can address multi-criteria optimization challenges for objective functions, that are expensive to evaluate. Nevertheless, Bayesian optimization is hardly used in the field of electrical machine design. Consequently, the present study explores the Bayesian multi-objective optimization methodology and discusses its application in terms of machine design. Employing four distinct acquisition functions, the study conducts three-objective optimization of a reluctance synchronous machine characterized by 14 design variables. Comparative analysis with NSGA-II reveals significantly superior outcomes achieved in a considerably shortened timeframe

Index Terms

Design optimization, electric machines, reluctance synchronous machine, Gaussian process regression, Bayesian optimization, expected hypervolumen improvement, expected improvement matrix, multi-objective optimization

NOTATION

$\mathbb{N}, \mathbb{R}$: Natural, real numbers. $\boldsymbol{x} := (x_1, \ldots, x_n)^\top \in \mathbb{R}^n$: Column vector, $n \in \mathbb{N}$ where "$^\top$" and ":=" mean "transposed" and "is defined as", respectively. $\boldsymbol{x}^\top \boldsymbol{y} := x_1 y_1 + \cdots + x_n y_n$: Scalar product of vectors $\boldsymbol{x}$ and $\boldsymbol{y}$. $\|\boldsymbol{x}\| := \sqrt{\boldsymbol{x}^\top \boldsymbol{x}} = \sqrt{x_1^2 + \cdots + x_n^2}$: Euclidean norm of $\boldsymbol{x}$. $\boldsymbol{X} \in \mathbb{R}^{n \times m}$: Matrix with n rows and m columns. $\|\boldsymbol{X}\| := \sup\{\|\boldsymbol{X}\boldsymbol{z}\| \mid \boldsymbol{z} \in \mathbb{R}^m \text{ with } \|\boldsymbol{z}\| = 1\}$: induced matrix 2-norm of $\boldsymbol{X}$. $|\boldsymbol{X}| \in \mathbb{R}^{n \times m}$: cardinality of set $\boldsymbol{X}$. $\boldsymbol{I}_n \in \mathbb{R}^{n \times n} := \mathrm{diag}(1, \ldots, 1)$: Identity matrix.

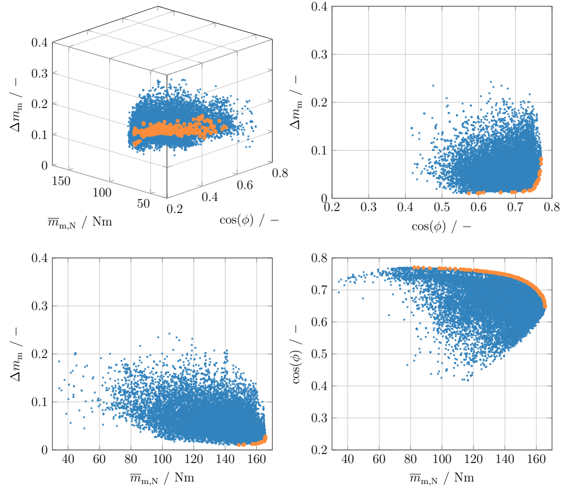

Fig. 7: Visualization of the three (unnormalized) objectives mean torque $\overline{m}_{\mathrm{m,N}}$, torque ripple Δm_m and power factor $\cos(\phi)$ of all 14.000 design evaluations (blue) and the corresponding 3D, respective 2D, Pareto fronts (orange).

Introduction

LMRES – Selected research results: Wind energy systems & power electronics (reliability; VDE Award) [78]

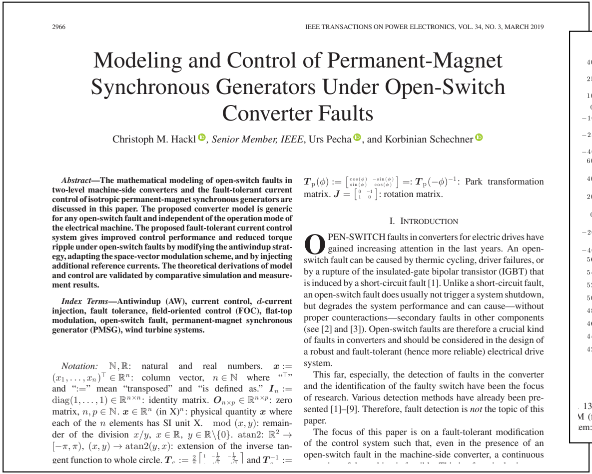

2966 IEEE TRANSACTIONS ON POWER ELECTRONICS, VOL. 34, NO. 3, MARCH 2019

Modeling and Control of Permanent-Magnet Synchronous Generators Under Open-Switch Converter Faults

Christoph M. Hackl, *Senior Member, IEEE*, Urs Pecha, and Korbinian Schechner

***Abstract*—The mathematical modeling of open-switch faults in two-level machine-side converters and the fault-tolerant current control of isotropic permanent-magnet synchronous generators are discussed in this paper. The proposed converter model is generic for any open-switch fault and independent of the operation mode of the electrical machine. The proposed fault-tolerant current control system gives improved control performance and reduced torque ripple under open-switch faults by modifying the antiwindup strategy, adapting the space-vector modulation scheme, and by injecting additional reference currents. The theoretical derivations of model and control are validated by comparative simulation and measurement results.**

***Index Terms*—Antiwindup (AW), current control, *d*-current injection, fault tolerance, field-oriented control (FOC), flat-top modulation, open-switch fault, permanent-magnet synchronous generator (PMSG), wind turbine systems.**

Notation: $\mathbb{N}, \mathbb{R}$: natural and real numbers. $\boldsymbol{x} := (x_1, \ldots, x_n)^\top \in \mathbb{R}^n$: column vector, $n \in \mathbb{N}$ where "$^\top$" and ":=" mean "transposed" and "is defined as." $\boldsymbol{I}_n := \mathrm{diag}(1, \ldots, 1) \in \mathbb{R}^{n \times n}$: identity matrix. $\boldsymbol{O}_{n \times p} \in \mathbb{R}^{n \times p}$: zero matrix, $n, p \in \mathbb{N}$. $\boldsymbol{x} \in \mathbb{R}^n$ (in X)^n: physical quantity $\boldsymbol{x}$ where each of the n elements has SI unit X. $\bmod\,(x, y)$: remainder of the division x/y, $x \in \mathbb{R}$, $y \in \mathbb{R}\backslash\{0\}$. atan2: $\mathbb{R}^2 \to [-\pi, \pi)$, $(x, y) \to \mathrm{atan2}(y, x)$: extension of the inverse tangent function to whole circle. $\boldsymbol{T}_c := \frac{2}{3}\left[\begin{smallmatrix} 1 & -\frac{1}{2} & -\frac{1}{2} \\ \ldots \end{smallmatrix}\right]$ and $\boldsymbol{T}_c^{-1} :=$

$\boldsymbol{T}_p(\phi) := \left[\begin{smallmatrix} \cos(\phi) & -\sin(\phi) \\ \sin(\phi) & \cos(\phi) \end{smallmatrix}\right] =: \boldsymbol{T}_p(-\phi)^{-1}$: Park transformation matrix. $\boldsymbol{J} = \left[\begin{smallmatrix} 0 & -1 \\ 1 & 0 \end{smallmatrix}\right]$: rotation matrix.

I. Introduction

OPEN-SWITCH faults in converters for electric drives have gained increasing attention in the last years. An open-switch fault can be caused by thermic cycling, driver failures, or by a rupture of the insulated-gate bipolar transistor (IGBT) that is induced by a short-circuit fault [1]. Unlike a short-circuit fault, an open-switch fault does usually not trigger a system shutdown, but degrades the system performance and can cause—without proper counteractions—secondary faults in other components (see [2] and [3]). Open-switch faults are therefore a crucial kind of faults in converters and should be considered in the design of a robust and fault-tolerant (hence more reliable) electrical drive system.

This far, especially, the detection of faults in the converter and the identification of the faulty switch have been the focus of research. Various detection methods have already been presented [1]–[9]. Therefore, fault detection is *not* the topic of this paper.

The focus of this paper is on a fault-tolerant modification of the control system such that, even in the presence of an open-switch fault in the machine-side converter, a continuous

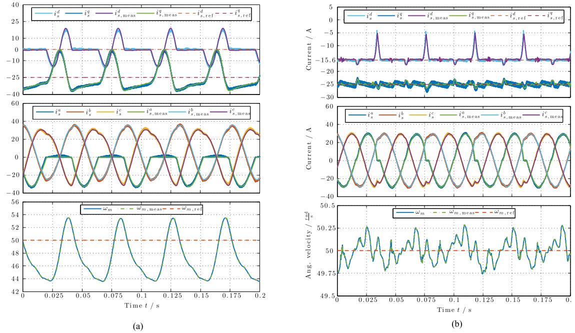

. 13. Comparison of simulation and measurement results for standard control system and fault-tolerant control system with extended AW, modifi M (flat-top modulation), and optimally injected d-current. (a) Experiment (E_1): Comparison of simulation and measurement results for standard contr em: $\mathrm{THD}_{i_s^a} = 41.8\,\%$ (simulation) versus $\mathrm{THD}_{i_s^a,\mathrm{meas}} = 45.4\,\%$ (measurement). (b) Experiment (E_2): Comparison of simulation and measurement resu

Introduction

LMRES – Selected research results: Wind energy systems & power electronics (grid stability, VSM) [169]

Industrial Electronics Society

Received 15 November 2023; revised 22 January 2024; accepted 5 February 2024. Date of publication 14 February 2024; date of current version 15 April 2024. The review of this article was arranged by Associate Editor Xing Zhao.

Digital Object Identifier 10.1109/OJIES.2024.3366082

Virtual Synchronous Machine Control for Doubly Fed Induction Machine-Based Wind Energy Conversion Systems

ANDRE THOMMESSEN (Member, IEEE) AND CHRISTOPH MICHAEL HACKL (Senior Member, IEEE)

Laboratory for Mechatronic and Renewable Energy Systems (LMRES), Hochschule München (HM) University of Applied Sciences, 80335 Munich, Germany

CORRESPONDING AUTHOR: CHRISTOPH M. HACKL (e-mail: christoph.hackl@hm.edu)

This work was financially supported by the Munich University of Applied Sciences HM and the Deutsche Forschungsgemeinschaft (DFG, German Research Foundation) under Grant 512819356 and was supported by the Federal Ministry for Economic Affairs and Climate Action of Germany under Grant 03EI6020B.

ABSTRACT Renewable inverter-based resources (IBRs), such as wind energy conversion systems (WSs), replace directly grid-connected synchronous machines (SMs). Standard grid-following (GFL) control of IBRs decreases the power system inertia. This article proposes virtual synchronous machine (VSM)-based grid-forming (GFM) control for doubly fed induction machine (DFIM)-based WSs with the following extensions: feedforward torque control (FTC) for maximum power point tracking (MPPT), MPPT compensation for accurate inertia emulation, reference power point tracking to provide energy reserves, dynamic droop saturation control to mitigate power overloading, and grid voltage control utilizing DFIM stator and rotor-side back-to-back inverter reactive power. The WSs are integrated into the IEEE 9-bus test system. Comprehensive simulation results give insights into (V)SM-based power system dynamics. Compared with existing VSM control without FTC, the proposed FTC increases the wind energy yield, i.e., typical MPPT performance is achieved, similar to GFL control. For high power penetration of IBRs, the proposed VSM control enables stable operation due to its GFM capability, whereas GFL control tends to instability. The VSM provides higher power system damping than a real SM due to adaptable internal damping. If wind power reserves are available, the fast VSM droop control provides additional damping by adapting the virtual turbine power without the dominant delays of real turbine dynamics.

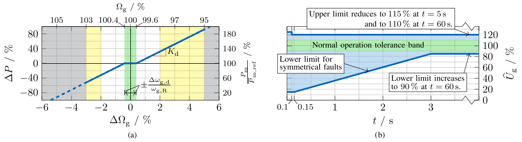

FIGURE 7. Illustration of German grid codes [36] with normal operation tolerance band [ ]. (a) Active power droop curve, as in (69), with extended admissible frequency range [ ], see also (R.5). (b) (Extended) Admissible voltage range [ ] with lower and upper fault-ride-through-curves [ ], see also Remark (R.8).

1) FEEDFORWARD TORQUE CONTROL

Assuming a grid-voltage-aligned dq-reference frame, the DFIM torque only depends on the d-component of the DFIM rotor current, recall (14), i.e., the FTC is given by

$$\boldsymbol{u}_s^{dq} = \begin{pmatrix} \widehat{u}_s \\ 0 \end{pmatrix} = \begin{pmatrix} \widehat{u}_g \\ 0 \end{pmatrix} \overset{(14)}{\Rightarrow} i^d_{r,\mathrm{ref}} := \frac{-X_s}{\kappa_p n_p M_{s,r} \widehat{u}_s} \overline{m}_{m,\mathrm{ref}} \quad (68)$$

with saturated torque reference $\overline{m}_{m,\mathrm{ref}}$ from (40), see Fig. 4.

2) DROOP CONTROL

The strategy is to primarily use the WS kinetic energy for inertia emulation, whereas droop control is only activated if additional energy reserves are available due to RPPT (instead of MPPT). This improves the WS stability (less severe WT speed nadir in Fig. 13) without degrading the grid support, as shown in the results later in Section IV-E2. If wind power reserves are available, i.e., for $P_{m,\mathrm{ref,rel}} < 1$ in (34), the WS has to provide droop power outside the tolerance band $\omega_{g,R} \pm \Delta\omega_{g,d}$ with rated grid angular velocity $\omega_{g,R}$ and tolerated grid angular velocity deviation $\pm\Delta\omega_{g,d}$ [36]. In Fig. 7(a), with droop gain k_d (see [2, Table X]) or normalized droop gain $K_d := k_d\omega_{g,R}$, the desired power change $\Delta P := (P_m - \overline{P}_{m,\mathrm{ref}})/\overline{P}_{m,\mathrm{ref}}$, relative to the power at rated grid frequency $P_m|_{\omega_g=\omega_{g,R}} = \overline{P}_{m,\mathrm{ref}}$ in (40), is given by [36]

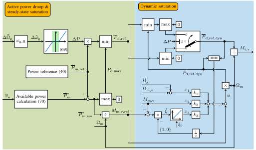

FIGURE 8. Active power droop control with overload protection.

the grid frequency if feasible. Moreover, GUs have to stay grid-connected within the range $2\pi 49 \frac{rad}{s} \le \omega_g \le 2\pi 51 \frac{rad}{s}$ or $98\% \le \Omega_g \le 102\%$, and, for a limited time interval of up to 30 min, GUs have to stay grid-connected within the extended range $2\pi 47.5 \frac{rad}{s} \le \omega_g \le 2\pi 51.5 \frac{rad}{s}$ or $95\% \le \Omega_g \le 103\%$, see [ ] in Fig. 7(a).[10]

In Fig. 8, the DFIM power reserve $\overline{P}^\star_{m,\mathrm{res}}$ is the difference between available $\overline{P}^\star_m$ and reference $\overline{P}_{m,\mathrm{ref}}$ DFIM power, leading to the maximum droop power $P_{d,\max}$ as follows:

Introduction

LMRES – Selected research results: Smart grid/renewables/power systems (grid synchronisation) [22]

Modified Second-Order Generalized Integrators With Modified Frequency Locked Loop for Fast Harmonics Estimation of Distorted Single-Phase Signals

Christoph M. Hackl, *Senior Member, IEEE*, and Markus Landerer

***Abstract*—This article proposes *modified second-order generalized integrators* (mSOGIs) for a fast estimation of all harmonic components of arbitrarily distorted single-phase signals, such as voltages or currents in power systems. The estimation is based on the internal model principle leading to an overall observer consisting of parallelized mSOGIs. The observer is tuned by pole placement. For a constant fundamental frequency, the observer is capable of estimating all harmonic components with prescribed settling time by choosing the observer poles appropriately. For time-varying fundamental frequencies, the harmonic estimation is combined with a *modified frequency locked loop* (mFLL) with gain normalization, sign-correct antiwindup, and rate limitation. The estimation performances of the proposed parallelized mSOGIs with and without mFLL are illustrated and validated by measurement results. The results are compared to standard approaches such as parallelized standard SOGIs (sSOGIs) and adaptive notch filters (ANFs).**

***Index Terms*—Amplitude estimation, frequency estimation, frequency-locked loop (FLL), phase estimation, second-order generalized integrator (SOGI).**

Notation

$\mathbb{N}, \mathbb{R}, \mathbb{C}, \mathbb{Q}$: natural, real, complex and rational numbers. For the following, let $n, m \in \mathbb{N}$. $\boldsymbol{x} := (x_1, \dots, x_n)^\top \in \mathbb{R}^n$: column vector (where := means "is defined as" and $^\top$ means "transposed"). $\boldsymbol{0}_n := (0, 0, \dots, 0)^\top \in \mathbb{R}^n$: zero vector. $\|\boldsymbol{x}\| := \sqrt{\boldsymbol{x}^\top \boldsymbol{x}}$: Euclidean norm of $\boldsymbol{x}$. $\boldsymbol{A} \in \mathbb{R}^{n \times m}$: real (non-square) matrix. $\mathrm{diag}(\boldsymbol{a}) \in \mathbb{R}^{n \times n}$: diagonal matrix with

I. Introduction

A. Motivation and Literature Review

In view of the increasing number of decentralized generation units with power electronics-based grid connection and the decreasing number of large-scale generators, the overall inertia in the grid is diminishing. This results in faster and more abrupt frequency fluctuations and significant harmonic distortion of physical quantities (such as currents or voltages) of the power system [1]. Fast frequency fluctuations endanger stability of the power grid. Significant harmonic distortions of voltages and currents can degrade power quality and lead to damage or even destruction of grid components. To be capable of taking appropriate countermeasures such as 1) improving system stability and power quality and 2) compensating for such deteriorated operation conditions, it is crucial to detect and estimate fundamental and higher harmonic components of the considered quantities in real time as fast and accurate as possible. Modern power electronic devices (e.g., flexible ac transmission systems or grid-connected converters of decentralized renewable energy systems) can then be used to implement such countermeasures. That is why, grid state estimation became of particular interest to the research community in the past years and has been studied extensively (see e.g., [2]–[24] to name a few).

It is well known that a signal with significant harmonic

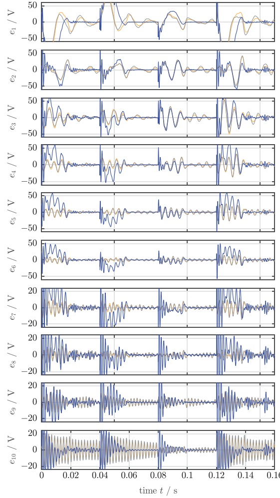

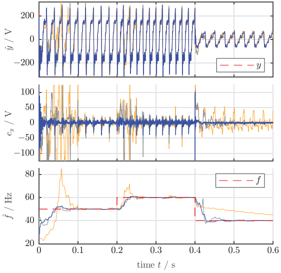

Fig. 11. Measurement results for Scenario (S_4): Comparison of the estimation performances of *parallelized* mSOGIs (—), sSOGIs (—), and ANFs (—) *without* FLL. Signals shown from top to bottom are: Harmonic signals y_1 to y_{10} (- - -) and their estimates $\widehat{y}_1$ to $\widehat{y}_{10}$ and harmonic estimation errors $e_1 = y_1 - \widehat{y}_1$ to $e_{10} = y_{10} - \widehat{y}_{10}$.

frequency are identical for this scenario. Therefore, the estimation performances purely can be compared according to the respective observer tunings only. The fundamental signal $y = y_1$ undergoes step-like changes in amplitude, phase and amplitude and phase as described above.

The estimation performances of fundamental mSOGI (—), fundamental sSOGI (—), and fundamental ANF (—) are shown in Fig. 7. The first and second subplots show input signal $y = y_1$ (- - -) and its estimates $\widehat{y} = \widehat{y}_1$ and the estimation errors $e_y = y_1 - \widehat{y}_1$, respectively. All three observers are capable of estimating the input signal y. All estimation errors $e_y \to 0$ tend to

Introduction

Frequency-adaptive pole placement [170]

Frequency-adaptive pole placement for parallelized proportional, integral and resonant control systems

Christoph Goettsberger and Christoph M. Hackl

Laboratory for Mechatronic and Renewable Energy Systems (LMRES)
Hochschule München (HM), University of Applied Sciences, Munich, Germany
{christoph.goettsberger, christoph.hackl}@hm.edu

***Abstract*—A novel and generic frequency-adaptive pole placement (FAPP) algorithm for parallelized proportional, integral and resonant (PIR) control systems is proposed. It allows to place arbitrarily many closed-loop poles at desired locations in the complex plane (usually negative complex half-plane) with individual damping and settling time characteristics. The closed-loop system with parallelized PIR controllers is then capable of tracking any linear combination of *constant* and *sinusoidal* reference signals asymptotically. The proposed FAPP algorithm achieves a better damped closed-loop system behaviour than Matlab's `place` command. Moreover, even when `place` fails to place the poles at the desired locations in the complex plane, the proposed FAPP will do the job. Additionally, the PIR controller is equipped with a simple anti-windup strategy and an effective reference feedforward control. The proposed approach is illustrated and validated by several simulation examples including multi-harmonic current control of a nonlinear electrical drive.**

***Index Terms*—frequency-adaptive pole placement, proportional, integral and resonant control**

Notation

$\mathbb{N}, \mathbb{R}, \mathbb{C}, \mathbb{Q}$: natural, real, complex and rational numbers. $\mathbb{R}_{\geq 0} := [0, \infty)$: positive real numbers with zero. $\mathbb{C}_{<0}$: negative complex half-plane, i.e., all $z \in \mathbb{C}_{<0}$ have negative real parts $\Re\{z\} < 0$. For the following, let $n \in \mathbb{N}$. $\boldsymbol{x} := (x_1, \cdots, x_n)^\top \in \mathbb{R}^n$: column vector (where $:=$ means "is defined as" and $^\top$ means "transposed"). $\boldsymbol{0}_n := (0, 0, , \cdots, 0)^\top \in \mathbb{R}^n$: zero vector. $\|\boldsymbol{x}\| := \sqrt{\boldsymbol{x}^\top \boldsymbol{x}}$: Euclidean norm of $\boldsymbol{x}$. $\boldsymbol{A} \in \mathbb{R}^{n \times m}$: real (non-square) matrix. $\boldsymbol{O}_{n \times m} \in \mathbb{R}^{n \times m}$: zero (non-square) matrix. $\boldsymbol{I}_n := \mathrm{diag}(\boldsymbol{1}_n) \in \mathbb{R}^{n \times n}$: identity matrix. $\boldsymbol{J} := \left[\begin{smallmatrix} 0 & -1 \\ 1 & 0 \end{smallmatrix}\right]$: rotation matrix rotating a vector by $\frac{\pi}{2}$ (counterclockwise).

I. Introduction

A. *Motivation*

Several applications require active control of constant and

reference signal containing not only constant terms but also multiple sinusoidal components. After Clarke transformation with Clarke transformation factor $\kappa \in \{\frac{2}{3}, \sqrt{\frac{2}{3}}\}$ (allowing for amplitude or power invariant transformation [12, Section 14.2.4]), such a time-varying reference signal $\boldsymbol{y}_{\mathrm{ref}}(t) := \boldsymbol{y}^{\alpha\beta}_{\mathrm{ref}}(t)$ in the (α, β)-reference frame[1] is given by

$$\boldsymbol{y}_{\mathrm{ref}}(t) = \underbrace{\begin{pmatrix} A^{\alpha}_{\mathrm{dc}}(t) \\ A^{\beta}_{\mathrm{dc}}(t) \end{pmatrix}}_{=:\boldsymbol{y}^{\alpha\beta}_{\mathrm{dc,ref}}(t)\ \text{[dc part]}} + \underbrace{\sum_{\nu \in \mathbb{H}} \overbrace{\tfrac{3}{2\kappa} A_\nu(t) \begin{pmatrix} \cos(\phi_\nu(t) + \varphi_\nu) \\ \sin(\phi_\nu(t) + \varphi_\nu) \end{pmatrix}}^{=:\boldsymbol{y}^{\alpha\beta}_{\nu,\mathrm{ref}}(t)}}_{=:\boldsymbol{y}^{\alpha\beta}_{\mathrm{ac,ref}}(t)\ \text{[ac part (harmonics)]}}. \tag{1}$$

It consists of desired dc reference $\boldsymbol{y}^{\alpha\beta}_{\mathrm{dc,ref}}(t)$ with possibly time-varying individual dc components $A^{\alpha}_{\mathrm{dc}}(t)$ and $A^{\beta}_{\mathrm{dc}}(t)$ and desired sinusoidal reference $\boldsymbol{y}^{\alpha\beta}_{\mathrm{ac,ref}}(t) = \sum_{\nu \in \mathbb{H}} \boldsymbol{y}^{\alpha\beta}_{\nu,\mathrm{ref}}(t)$ with a possibly time-varying amplitude $A_\nu(t)$, time-varying angle

$$\phi_\nu(t) := \int_0^t \nu \omega_{\mathrm{f}}(\tau)\,\mathrm{d}\tau \quad \text{with harmonic order } \nu \in \mathbb{H} \subset \mathbb{Q},$$

which depends on the time-varying fundamental angular frequency $\omega_{\mathrm{f}}(t)$, and constant phase offset φ_ν, respectively for each harmonic order $\nu \in \mathbb{H}$. The set $\mathbb{H}$ of harmonic orders may contain any rational numbers $\nu \in \mathbb{Q}$ including e.g. positive ($\nu_+ > 0$) and negative ($\nu_- < 0$) sequence harmonic orders.

The internal model principle [13], well known in control theory, states that for such reference (or disturbance) signals, a parallelization of proportional, integral and (multiple) resonant controllers ($\mathrm{PIR}_{\mathbb{H}}$ controller) is necessary to achieve asymptotic tracking by reduplicating the constant and sinusoidal components of all harmonic orders $\nu \in \mathbb{H}$ of the reference signal in (1). However, the tuning of the parallel $\mathrm{PIR}_{\mathbb{H}}$ controller

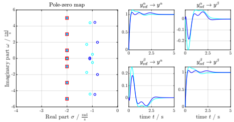

(a) $\mathbb{H}_1 := \{3; 5\}$ with $h_1 = 2$ and $m_1 = 8$.

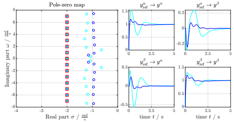

(b) $\mathbb{H} := \{2; 3; 4; 5; 6; 7\}$ with $h_2 = 6$ and $m_2 = 16$.

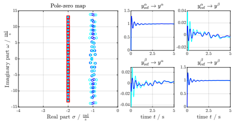

(c) $\mathbb{H}_3 := \{\pm 2; \pm 3; \pm 4; 5; -6; \pm 7; \pm 8; \pm 9; \pm 10; 11; -12; \pm 13\}$ with $h_3 = 20$ and $m_3 = 44$.

Figure 2: Illustrative simulation results for different harmonic set $\mathbb{H}$ (see subplots (a), (b) & (c)) and tuning according to **($\mathbf{ESG}_1$)** with `place` [—] and FAPP [—]: poles [×], zeros [○] & desired poles [□] (double pole on real axis in each subplot (a), (b) & (c)).

respectively. Pole placement with `place` (from Matlab) and FAPP are performed according to the Eigenvalue Selection Guidelines **($\mathbf{ESG}_1$)** and **($\mathbf{ESG}_2$)** (recall Section II-D3) and

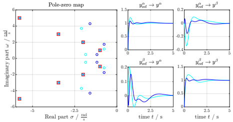

(a) $\mathbb{H}_1 := \{3; 5\}$ with $h_1 = 2$ and $m_1 = 8$.

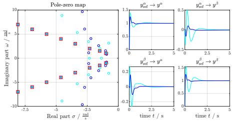

(b) $\mathbb{H}_2 := \{2; 3; 4; 5; 6; 7\}$ with $h_2 = 6$ and $m_2 = 16$.

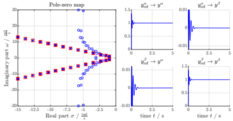

(c) $\mathbb{H}_3 := \{\pm 2; \pm 3; \pm 4; 5; -6; \pm 7; \pm 8; \pm 9; \pm 10; 11; -12; \pm 13\}$ with $h_3 = 20$ and $m_3 = 44$ ("`place`" **fails**; not shown here).

Figure 3: Illustrative simulation results for different harmonic set $\mathbb{H}$ (see subplots (a), (b) & (c)) and tuning according to **($\mathbf{ESG}_2$)** with `place` [—] and FAPP [—]: poles [×], zeros [○] & desired poles [□].

when compared with the desired Eigenvalues highlighted by red squares [□]. The respective step responses are also simular; however, the closed-loop systems tuned by `place` (see cyan lines [—]) exhibit more oscillations and are less well damped

Introduction

Motivation and problem statement

Reference signal with constant and (multiple) sinusoidal components

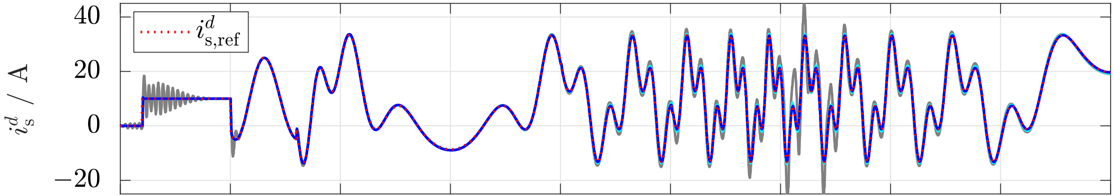

Can we achieve fast and accurate tracking ...

- with (almost) no overshoot ?
- with (asymptotically) vanishing tracking error ?
- while considering multiple harmonics and dc-offsets ?
- by which controller structure ?
- by which tuning even if the frequency is varying ?

Proposed controller structure

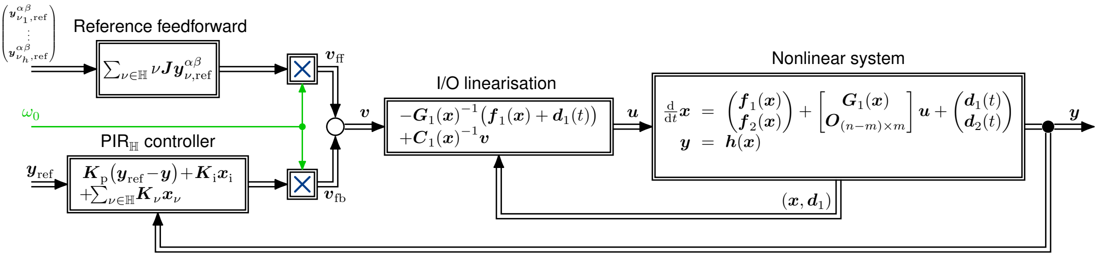

for **frequency-adaptive pole placement for parallelized proportional, integral and resonant control systems**, which is conducted in four steps:

- Step 1: Input/output (I/O) linearization;
- Step 2: Implementation of parallelized PIR$_{\mathbb{H}}$ controller;
- Step 3: Frequency-adaptive pole placement; and
- Step 4: Reference feedforward control.

Considered system class with multi-input $\boldsymbol{u} \in \mathbb{R}^m$ multi-ouput $\boldsymbol{y} \in \mathbb{R}^m$ (MIMO) dynamics

$$\left.\begin{aligned} \frac{\mathrm{d}}{\mathrm{d}t}\boldsymbol{x} &= \begin{pmatrix} \boldsymbol{f}_1(\boldsymbol{x}) \\ \boldsymbol{f}_2(\boldsymbol{x}) \end{pmatrix} + \begin{bmatrix} \boldsymbol{G}_1(\boldsymbol{x}) \\ \boldsymbol{O}_{(n-m)\times m} \end{bmatrix} \boldsymbol{u} + \begin{pmatrix} \boldsymbol{d}_1(t) \\ \boldsymbol{d}_2(t) \end{pmatrix} \\ \boldsymbol{y} &= \boldsymbol{h}(\boldsymbol{x}) \end{aligned}\right\} \tag{1}$$

where $\boldsymbol{f}_1 \colon \mathbb{R}^n \to \mathbb{R}^m$, $\boldsymbol{f}_2 \colon \mathbb{R}^n \to \mathbb{R}^{n-m}$, $\boldsymbol{h} \colon \mathbb{R}^n \to \mathbb{R}^m$, $\boldsymbol{G}_1 \colon \mathbb{R}^n \to \mathbb{R}^{m\times m}$ with $\det \boldsymbol{G}_1(\boldsymbol{x}) \neq 0$ and

$$\left[\frac{\mathrm{d}}{\mathrm{d}\boldsymbol{x}}\boldsymbol{h}(\boldsymbol{x})\right]^\top = \Big[\underbrace{\frac{\mathrm{d}}{\mathrm{d}(x_1,\ldots,x_m)}\boldsymbol{h}(\boldsymbol{x}),}_{=:\boldsymbol{C}_1(\boldsymbol{x})\in\mathbb{R}^{m\times m}} \quad \boldsymbol{O}_{m\times(n-m)}\Big]$$

with $\det \boldsymbol{C}_1(\boldsymbol{x}) \neq 0$ for all $\boldsymbol{x} \in \mathbb{R}^n$ (i.e., $\boldsymbol{G}_1(\boldsymbol{x})$ and $\boldsymbol{C}_1(\boldsymbol{x})$ are invertible).

Step 1: Input/output (I/O) linearization

$$\boxed{\boldsymbol{u} = -\boldsymbol{G}_1(\boldsymbol{x})^{-1}\big(\boldsymbol{f}_1(\boldsymbol{x}) + \boldsymbol{d}_1(t) + \boldsymbol{C}_1(\boldsymbol{x})^{-1}\boldsymbol{v}\big),} \tag{2}$$

gives $\frac{\mathrm{d}}{\mathrm{d}t}\boldsymbol{y} \overset{(1),(2)}{=} \boldsymbol{C}_1(\boldsymbol{x})\Big[\boldsymbol{f}_1(\boldsymbol{x}) + \boldsymbol{G}_1(\boldsymbol{x}) \cdot \Big(-\boldsymbol{G}_1(\boldsymbol{x})^{-1}\big(\boldsymbol{f}_1(\boldsymbol{x}) + \boldsymbol{d}_1(t) + \boldsymbol{C}_1(\boldsymbol{x})^{-1}\boldsymbol{v}\big)\Big) + \boldsymbol{d}_1(t)\Big] = \boldsymbol{v}$.

Frequency-adaptive pole placement for parallelized systems

Step 2: Implementation of parallelized $\mathrm{PIR}_{\mathbb{H}}$ controller

Properties of controller:

- Let $m=2 \to 2$-input, 2-output system of form (1)
- Choose set $\mathbb{H}$ of harmonic orders with cardinality $|\mathbb{H}| =: h \in \mathbb{N}$
- Choose the $\mathrm{PIR}_{\mathbb{H}}$ controller's feedback vector $\boldsymbol{v}_{\mathrm{fb}} \in \mathbb{R}^2$ with $2h+2$ states $\boldsymbol{x}_{\mathrm{pir}} := (\boldsymbol{x}_{\mathrm{i}}^\top, \boldsymbol{x}_{\nu_1}^\top, \cdots, \boldsymbol{x}_{\nu_h}^\top)^\top \in \mathbb{R}^{2h+2}$, including integral states $\boldsymbol{x}_{\mathrm{i}} \in \mathbb{R}^2$ and h resonant double states $\boldsymbol{x}_\nu \in \mathbb{R}^2$ for all $\nu \in \mathbb{H}$.

Hence, the **parallelized $\mathrm{PIR}_{\mathbb{H}}$ controller** is given by

$$\left.\begin{aligned}
\boldsymbol{v}_{\mathrm{fb}} &= \omega_0\Big[\boldsymbol{K}_{\mathrm{p}}\big(\boldsymbol{y}_{\mathrm{ref}}-\boldsymbol{y}\big)+\boldsymbol{K}_{\mathrm{i}}\boldsymbol{x}_{\mathrm{i}}+\sum_{\nu\in\mathbb{H}}\boldsymbol{K}_{\nu}\boldsymbol{x}_{\nu}\Big]\\
\frac{\mathrm{d}}{\mathrm{d}t}\boldsymbol{x}_{\mathrm{pir}} &= \underbrace{\omega_0\overbrace{\begin{bmatrix}\boldsymbol{O} & \boldsymbol{O} & \cdots & \boldsymbol{O}\\ \boldsymbol{O} & \nu_1\boldsymbol{J} & \ddots & \vdots\\ \vdots & \ddots & \ddots & \boldsymbol{O}\\ \boldsymbol{O} & \cdots & \boldsymbol{O} & \nu_h\boldsymbol{J}\end{bmatrix}}^{=:\boldsymbol{A}_{\mathrm{pir}}}\boldsymbol{x}_{\mathrm{pir}}+\omega_0\overbrace{\begin{bmatrix}\boldsymbol{I}_2\\ \boldsymbol{I}_2\\ \vdots\\ \boldsymbol{I}_2\end{bmatrix}}^{=:\boldsymbol{B}_{\mathrm{pir}}}\big(\boldsymbol{y}_{\mathrm{ref}}-\boldsymbol{y}\big)}_{=:\boldsymbol{f}_{\mathrm{pir}}(\boldsymbol{x}_{\mathrm{pir}},\boldsymbol{y}_{\mathrm{ref}}-\boldsymbol{y},\omega_0,\omega_{\mathrm{i}},\omega_{\mathrm{f}},\ldots,\omega_{\nu_h})}
\end{aligned}\right\} \tag{3}$$

Remark: Note that all gain matrices $\boldsymbol{K}_{\mathrm{p}}$, $\boldsymbol{K}_{\mathrm{i}}$ and $\boldsymbol{K}_{\nu_1}, \ldots, \boldsymbol{K}_{\nu_h}$ are element of $\mathbb{R}^{2\times 2}$ and may be scaled by some angular frequency $\omega_0 \geq 1$. Anti-windup should also be implemented.

Frequency-adaptive pole placement for parallelized systems

Step 3: Frequency-adaptive pole placement

The **frequency-adaptive tuning rule for the controller gain matrices**

$$\boldsymbol{K} := \left[-\boldsymbol{K}_{\mathrm{p}}, \quad \boldsymbol{K}_{\mathrm{i}}, \quad \boldsymbol{K}_{\nu_1}, \quad \cdots, \quad \boldsymbol{K}_{\nu_h}\right] \in \mathbb{R}^{2\times m} \tag{4}$$

is obtained as

$$\boldsymbol{K} = \left[\boldsymbol{\Lambda}^\star_{\mathbb{R},1} \quad \cdots \quad \boldsymbol{\Lambda}^\star_{\mathbb{R},l}\right] \begin{bmatrix} \boldsymbol{I}_2 & \cdots & \boldsymbol{I}_2 \\ \boldsymbol{T}_{2,1} & \cdots & \boldsymbol{T}_{2,l} \\ \vdots & \ddots & \vdots \\ \boldsymbol{T}_{l,1} & \cdots & \boldsymbol{T}_{l,l} \end{bmatrix}^{-1} \quad \text{with } \boldsymbol{\Lambda}^\star_{\mathbb{R},k} := \begin{bmatrix} -\sigma^\star_k & -\omega^\star_k \\ \omega^\star_k & -\sigma^\star_k \end{bmatrix} = -\sigma^\star_k \boldsymbol{I}_2 + \omega^\star_k \boldsymbol{J}, \tag{5}$$

where, for all $i \in \{2, \cdots, l\}$ and $j \in \{1, \cdots, l\}$,

$$\boldsymbol{T}_{i,j} = \alpha_1 \left[\alpha_i \boldsymbol{J} - \boldsymbol{\Lambda}^\star_{\mathbb{R},j}\right]^{-1}. \tag{6}$$

Remark: The simple definition above is based on the introduction of $\alpha_1 := 1$, $\alpha_2 := 0$, $\alpha_3 := \nu_1$, $\alpha_4 := \nu_2, \ldots, \alpha_l := \nu_h$. All $\boldsymbol{T}_{i,j}$ depend solely on known quanteties such as the harmonic orders $\nu_1 = \alpha_3, \nu_2 = \alpha_4, \ldots, \nu_h = \alpha_l$, and real $\sigma^\star_j$ and imaginary $\omega^\star_j$ parts of the j-th desired pole pair $\lambda^\star_j = -\sigma^\star_j + \jmath\omega^\star_j$ and $\overline{\lambda}^\star_j = -\sigma^\star_j - \jmath\omega^\star_j$, respectively.

Frequency-adaptive pole placement for parallelized systems

Step 4: Reference feedforward control

Invoking the Internal Model Principle, the desired **reference feedforward control** has the following form

$$\boldsymbol{v}_{\mathrm{ff}} = \sum_{\nu\in\mathbb{H}} \omega_\nu \boldsymbol{J}\boldsymbol{y}^{\alpha\beta}_{\nu,\mathrm{ref}} = \omega_0 \sum_{\nu\in\mathbb{H}} \nu \boldsymbol{J}\boldsymbol{y}^{\alpha\beta}_{\nu,\mathrm{ref}}, \tag{7}$$

which only depends on the actual reference components of the respective harmonic order $\nu \in \mathbb{H}$. Combining all four steps gives the **overall control system** (as introduced above):

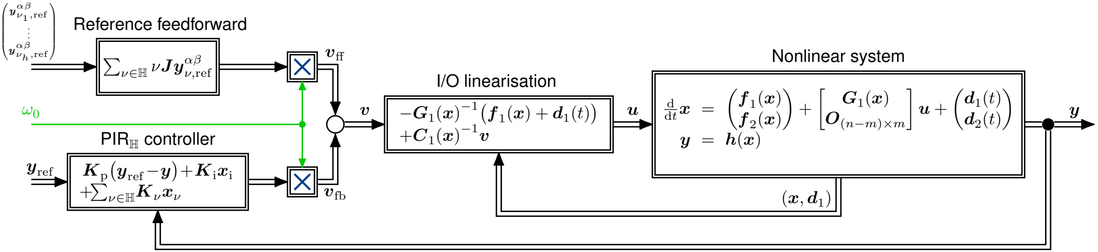

Implementation and simulative validation

Illustrative examples – Example 1: $\mathbb{H}_1 := \{3; 5\}$ with $h_1 = 2$ and $m_1 = 8$.

Considered simple dynamical system (pure integrator; e.g., after I/O linearization):

$$\frac{\mathrm{d}}{\mathrm{d}t}\boldsymbol{y} = \frac{\mathrm{d}}{\mathrm{d}t}\begin{pmatrix} y^{\alpha} \\ y^{\beta} \end{pmatrix} = \boldsymbol{u} := \begin{pmatrix} u^{\alpha} \\ u^{\beta} \end{pmatrix}$$

Eigenvalue Selection Guideline 1:

$$\sigma_j^\star = \alpha^\star \wedge \omega_j^\star = \nu_j^\star \Rightarrow \lambda_j^\star = -\alpha^\star \pm \jmath \nu_j^\star$$

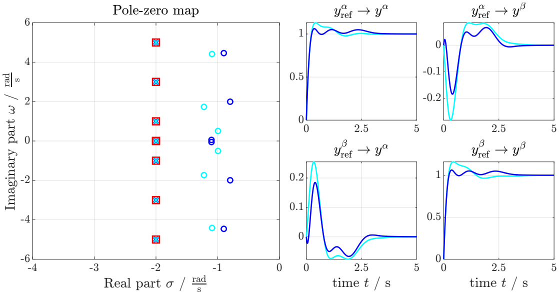

Eigenvalue Selection Guideline 2:

$$\sigma_j^\star = \frac{\nu_j^\star}{\sqrt{1-(D^\star)^2}} \wedge \omega_j^\star = \nu_j \Rightarrow \lambda_j^\star = -\nu_j^\star\left(\frac{1}{\sqrt{1-(D^\star)^2}} \pm \jmath\right)$$

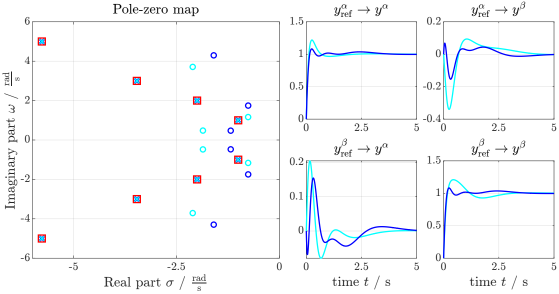

——————- Legend: `place` [—] and FAPP [—]: poles [×], zeros [○] ——————

Implementation and simulative validation

Illustrative examples – Example 2: $\mathbb{H}_2 := \{2; 3; 4; 5; 6; 7\}$ with $h_2 = 6$ and $m_2 = 16$.

Considered simple dynamical system (pure integrator; e.g., after I/O linearization):

$$\frac{\mathrm{d}}{\mathrm{d}t}\boldsymbol{y} = \frac{\mathrm{d}}{\mathrm{d}t}\begin{pmatrix} y^{\alpha} \\ y^{\beta} \end{pmatrix} = \boldsymbol{u} := \begin{pmatrix} u^{\alpha} \\ u^{\beta} \end{pmatrix}$$

Eigenvalue Selection Guideline 1:

$$\sigma_j^\star = \alpha^\star \wedge \omega_j^\star = \nu_j^\star \Rightarrow \lambda_j^\star = -\alpha^\star \pm \jmath \nu_j^\star$$

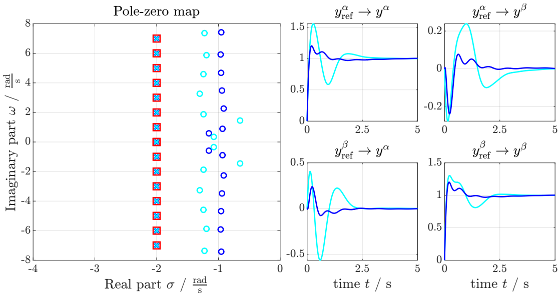

Eigenvalue Selection Guideline 2:

$$\sigma_j^\star = \frac{\nu_j^\star}{\sqrt{1-(D^\star)^2}} \wedge \omega_j^\star = \nu_j \Rightarrow \lambda_j^\star = -\nu_j^\star\left(\frac{1}{\sqrt{1-(D^\star)^2}} \pm \jmath\right)$$

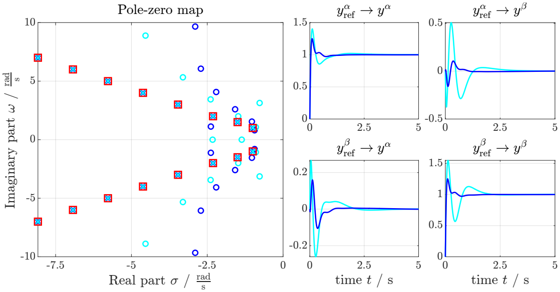

Legend: `place` [—] and FAPP [—]: poles [×], zeros [∘]

Implementation and simulative validation

Illustrative examples – Example 3: $\mathbb{H}_3 := \{\pm 2; \pm 3; \pm 4; 5; -6; \pm 7; \pm 8; \pm 9; \pm 10; 11; -12; \pm 13\}$ with $h_3 = 20$ and $m_3 = 44$

Considered simple dynamical system (pure integrator; e.g., after I/O linearization):

$$\frac{\mathrm{d}}{\mathrm{d}t}\boldsymbol{y} = \frac{\mathrm{d}}{\mathrm{d}t}\begin{pmatrix} y^{\alpha} \\ y^{\beta} \end{pmatrix} = \boldsymbol{u} := \begin{pmatrix} u^{\alpha} \\ u^{\beta} \end{pmatrix}$$

Eigenvalue Selection Guideline 1:

$$\sigma_j^{\star} = \alpha^{\star} \wedge \omega_j^{\star} = \nu_j^{\star} \Rightarrow \lambda_j^{\star} = -\alpha^{\star} \pm \jmath \nu_j^{\star}$$

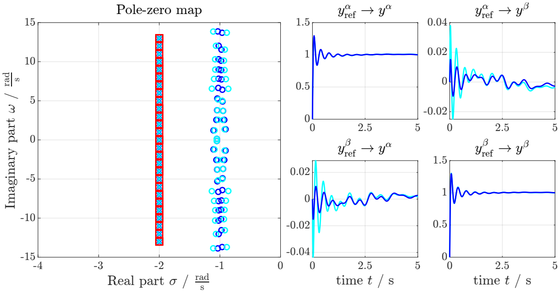

Eigenvalue Selection Guideline 2: ("`place`" fails!)

$$\sigma_j^{\star} = \frac{\nu_j^{\star}}{\sqrt{1-(D^{\star})^2}} \wedge \omega_j^{\star} = \nu_j \Rightarrow \lambda_j^{\star} = -\nu_j^{\star}\left(\frac{1}{\sqrt{1-(D^{\star})^2}} \pm \jmath\right)$$

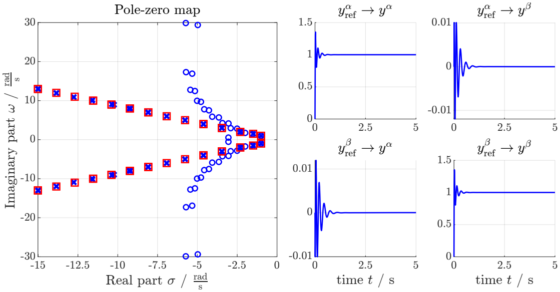

———— Legend: `place` [—] and FAPP [—]: poles [×], zeros [○] ————

Implementation and simulative validation

Multi-harmonic current control of nonlinear IPMSM – machine model

Nonlinear machine dynamics

$$\left.\begin{aligned}
\frac{\mathrm{d}}{\mathrm{d}t}\boldsymbol{i}_{\mathrm{s}}^{dq} &= \left(\boldsymbol{L}_{\mathrm{s}}^{dq}\right)^{-1}\left(\boldsymbol{u}_{\mathrm{s}}^{dq} - \boldsymbol{R}_{\mathrm{s}}^{dq}\boldsymbol{i}_{\mathrm{s}}^{dq} - n_{\mathrm{p}}\omega_{\mathrm{m}}\boldsymbol{J}\boldsymbol{\psi}_{\mathrm{s}}^{dq}\right)\\
\frac{\mathrm{d}}{\mathrm{d}t}\omega_{\mathrm{m}} &= \frac{1}{\Theta_{\mathrm{m}}}\left(m_{\mathrm{m}} - m_{\mathrm{l}}\right),\\
\frac{\mathrm{d}}{\mathrm{d}t}\phi_{\mathrm{m}} &= \omega_{\mathrm{m}}.
\end{aligned}\right\} \tag{8}$$

with nonlinear flux linkage maps

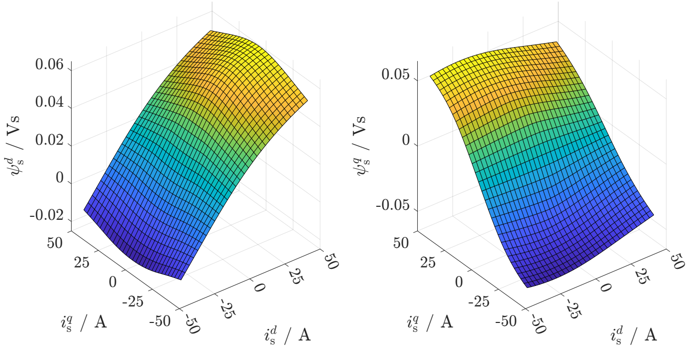

Implementation and simulative validation

Multi-harmonic current control of nonlinear IPMSM

Controller specifications / tuning:

- Desired harmonics $\mathbb{H}_{\mathrm{ipmsm}} := \{1; 3\} \Rightarrow$ number of harmonics $h_{\mathrm{ipmsm}} = 2$ and states $m_{\mathrm{ipmsm}} = 8$;
- Pole placement with (unscaled) desired poles $\sigma_j^\star$, $\omega_j^\star$ as in figure below (see [])
- Varying speeds $\Rightarrow$ frequency adaptation $\alpha_{\mathrm{m}} n_{\mathrm{p}} \omega_{\mathrm{m,R}} \left(\beta_{\mathrm{m}} + \frac{|\omega_{\mathrm{m}}(t)|}{\omega_{\mathrm{m,R}}}\right)$ with $\alpha_{\mathrm{m}} = 1$ and $\beta_{\mathrm{m}} = 0.05$

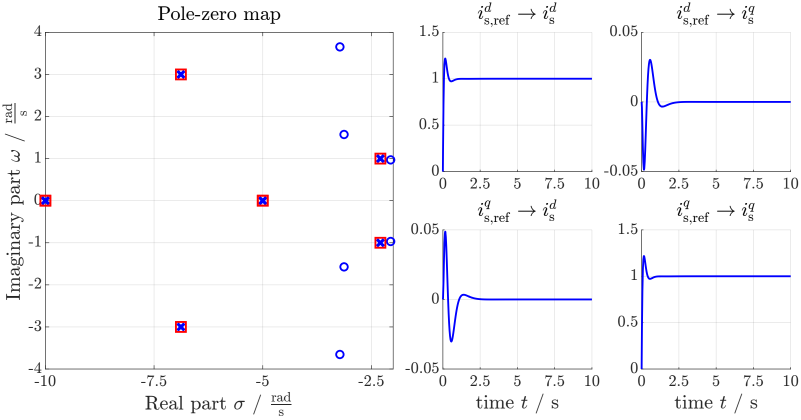

Implementation and simulative

Multi-harmonic current control of nonlinear IPMSM

High-fidelity simulation results:
Three different controller implementations to compare multi-harmonic current control performace for nonlinear IPMSM:

(C1) $\text{PIR}_{\mathbb{H}}$ controller *without* reference feedforward control and *without* frequency adaption (w/o RFF & w/o FA) [—];

(C2) $\text{PIR}_{\mathbb{H}}$ controller *without* reference feedforward control but *with* frequency adaption (w/o RFF & w/ FA) [—] and

(C3) $\text{PIR}_{\mathbb{H}}$ controller *with* reference feedforward control and *with* frequency adaption (w/ RFF & w/ FA) [—]

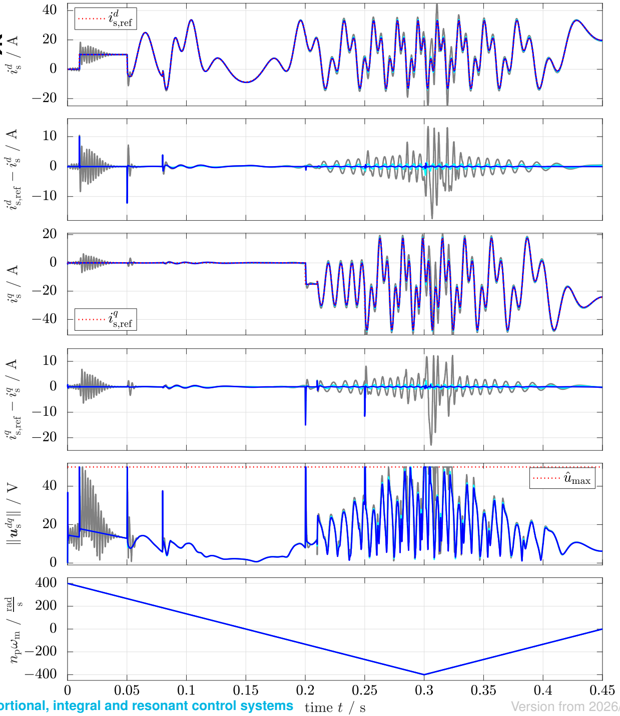

Outlook

FAPP application and combination with frequency adaptive observer (FAO) for active power filter (APF) control [171]

ence of the IEEE Industrial Electronics Society | 979-8-3315-9681-1/25/$31.00 ©2025 IEEE | DOI: 10.1109/IECON58223.2025.11221362

A generic observer-based control system for three-phase parallel active power filters

1st Christoph Göttsberger†, 2nd Dietmar Fehrenbach‡, 3rd Marek Galek‡ and 4th Christoph M. Hackl†,⋆
Laboratory for Mechatronic and Renewable Energy Systems (LMRES)†, *Laboratory for Power Electronics (LLE)*‡
Hochschule München (HM) University of Applied Sciences
Munich, Germany
{christoph.goettsberger, dietmar.fehrenbach, marek.galek, christoph.hackl}@hm.edu (⋆corresponding author)

***Abstract*—Parallel active power filters (PAPF) compensate for current harmonics and grid imbalances caused by (active or passive) nonlinear loads or sources. The proposed novel approach for controlling PAPFs is based on a combination of (i) frequency-adaptive observers for grid voltages and (load) currents, (ii) computation of the PAPF reference currents based on these observed quantities and (pre-)specified filter goals, and (iii) multi-harmonic current control tuned by frequency-adaptive pole placement. The proposed approach achieves grid current harmonic mitigation, load current balancing, and power factor correction. Observers and controllers may adapt themselves to the fundamental grid frequency. High-fidelity simulations of a real-world application show the effectiveness and achievable filtering performance of this overall observer-based control system.**

***Index Terms*—frequency-adaptive observer; proportional, integral & resonant control; parallel active power filter; harmonic mitigation; load balancing; power factor correction.**

NOTATION

$\mathbb{N}, \mathbb{R}, \mathbb{C}, \mathbb{Q}$: natural, real, complex and rational numbers. $\mathbb{C}_{<0}$: negative complex half-plane, i.e., all $z \in \mathbb{C}_{<0}$ have negative real parts $\Re\{z\} < 0$. For the following, let $n \in \mathbb{N}$. $\boldsymbol{x} := (x_1, \cdots, x_n)^\top \in \mathbb{R}^n$: column vector (where $:=$ means "is defined as" and $^\top$ means "transposed"). $\boldsymbol{0}_n := (0, 0, \cdots, 0)^\top \in \mathbb{R}^n$: zero vector. $\|\boldsymbol{x}\| := \sqrt{\boldsymbol{x}^\top \boldsymbol{x}}$: Euclidean norm of $\boldsymbol{x}$. $\boldsymbol{A} \in \mathbb{R}^{n\times m}$: real (non-square) matrix. $\boldsymbol{O}_{n\times m} \in \mathbb{R}^{n\times m}$: zero (non-square) matrix. $\boldsymbol{I}_n := \mathrm{diag}(\boldsymbol{1}_n) \in \mathbb{R}^{n\times n}$: identity matrix. $\boldsymbol{J} := \left[\begin{smallmatrix}0 & -1\\ 1 & 0\end{smallmatrix}\right]$: rotation matrix rotating a vector by $\frac{\pi}{2}$ (counterclockwise). $a \overset{!}{=} b$: a should equal b. $\boldsymbol{A} \otimes \boldsymbol{B}$: Kronecker product of $\boldsymbol{A}$ & $\boldsymbol{B}$ [1, Definition 7.1.2].

I. INTRODUCTION

Motivation and problem statement: Parallel active power

the reference currents to achieve the desired filtering behavior.

State of the art: Various methods for the determination of filter reference currents are reviewed in [2] and [5]. Classical methods for filter reference current computation are divided into time-domain and frequency-domain-based methods, each with their own advantages and disadvantages. Frequency domain and Fourier transform based methods like FFT/DFT or recursive DFT [6] are sufficient for frequency component separation but are sensitive to incompletely sampled time periods (resulting in poor harmonic resolution) and, depending on their implementation, are not necessarily suitable for real-time applications, according to [7]. Nevertheless, as was shown in [8], these approaches allow for an explicit selection of frequency components (which should be compensated for) and the proper determination of filter reference currents. Time-domain-based approaches are typically either based on the instantaneous p-q-theory (e.g., [9]) or on considerations in synchronously rotating (d, q)-reference frames [10]. As summarized in [11], these reference current generation techniques require modifications under unbalanced and distorted grid voltages to achieve adequate filtering objectives. Other time domain approaches are based on the stationary (α, β)-reference frame. In particular, generalized integrators are used for (a) positive- and negative sequence separation [12], (b) robustness against grid harmonics and imbalances [13] and (c) extraction of fundamental grid voltage and load current components [14]. Common to all these approaches is a quasi-instantaneous and real-time capable determination of the fundamental frequency components, without frequency selective extraction of non-fundamental load current components. As

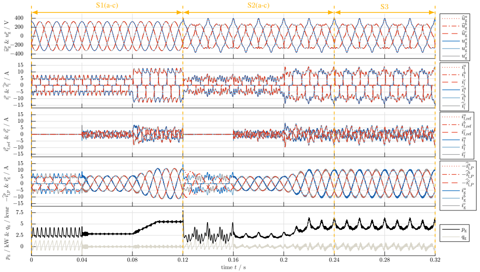

Figure 5: High-fidelity simulation results of proposed observer-based control system for PAPF (as in Fig. 4) under varying grid and load conditions: The considered simulation Scenarios S1-S3 are described in detail in Table II.

Scenario	S1(a)	S1(b)	S1(c)	S3(a)	S3(b)	S3(c)	S4	
t / 40 ms	[0; 1)	[1; 2)	[2; 3)	[3; 4)	[4; 5)	[5; 6)	[6; 7)	[7; 8)
PAPF turned on	0	1	1	0	1	1	1	1
R_l / $R_{l,1}$	1	1	2	1	1	2	2	2
$\boldsymbol{u}^{\alpha\beta}_{g(0)\pm}$ / 16.25 V	$(0\quad 0)^\top$			$(1\quad 0)^\top$				
$\boldsymbol{u}^{\alpha\beta}_{g(1)\pm}$ / 325 V	$(1\quad 0)^\top$			$(0.9\quad 0.1)^\top$				
$\boldsymbol{u}^{\alpha\beta}_{g(2)\pm}$ / 6.5 V	$(0\quad 0)^\top$			$(1\quad 0)^\top$				
$\boldsymbol{u}^{\alpha\beta}_{g(3)\pm}$ / 16.25 V	$(0\quad 0)^\top$			$(1\quad 0)^\top$				
$\boldsymbol{u}^{\alpha\beta}_{g(4)\pm}$ / 3.25 V	$(0\quad 0)^\top$			$(1\quad 0)^\top$				
$\boldsymbol{u}^{\alpha\beta}_{g(5)\pm}$ / 19.5 V	$(0\quad 0)^\top$			$(1\quad 0)^\top$				
$\boldsymbol{u}^{\alpha\beta}_{g(6)\pm}$ / 1.625 V	$(0\quad 0)^\top$			$(1\quad 0)^\top$				
$\boldsymbol{u}^{\alpha\beta}_{g(7)\pm}$ / 16.25 V	$(0\quad 0)^\top$			$(1\quad 0)^\top$				
$\boldsymbol{u}^{\alpha\beta}_{g(8)\pm}$ / 1.625 V	$(0\quad 0)^\top$			$(1\quad 0)^\top$				
$\boldsymbol{u}^{\alpha\beta}_{g(9)\pm}$ / 4.875 V	$(0\quad 0)^\top$			$(1\quad 0)^\top$				
$\boldsymbol{u}^{\alpha\beta}_{g(10)\pm}$ / 1.625 V	$(0\quad 0)^\top$			$(1\quad 0)^\top$				

Table II: Sim. scenarios with varying grid & load conditions.

grid currents $\boldsymbol{i}_g^{abc}$ have almost perfect fundamental sinusoidal shape. The high-frequency deviations are due to the switching nature of the PAPF and may be reduced even further by choosing an even higher switching frequency f_{sw}. During S2, due to the unbalanced grid voltages $\boldsymbol{u}_g^{abc}$ polluted by several harmonics as well as zero, positive, and negative sequence components (see Tab. II), the instantaneous active p_g and reactive q_g grid powers contain the grid harmonics as well. Scenario S3 allows to analyze the (quasi-)steady-state performance of the PAPF, which is illustrated by the FFT

of load and grid currents. Compared to the resulting grid currents, the load currents of each phase $p \in \{a, b, c\}$ contain, due to the nonlinear load, many more and less damped harmonic components $I^p_{l(\nu)}$ and $I^p_{g(\nu)}$ besides their fundamental components $I^p_{l(1)}$ and $I^p_{g(1)}$, respectively. For example, the load currents may contain third $I^p_{l(3)}$, fifth $I^p_{l(5)}$, seventh $I^p_{l(7)}$, ninth $I^p_{l(9)}$ and eleventh $I^p_{l(11)}$ harmonic components, whereas those (and also all other harmonic components) of the grid currents are filtered out by the PAPF at least by 40 dB.

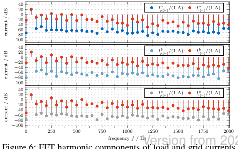

Figure 6: FFT harmonic components of load and grid currents

Conclusion

To take home

- Novel and generic frequency-adaptive pole placement (FAPP) algorithm (beats `place`!)
- Applicable for for parallelized proportional, integral and resonant (PIR) control systems has been presented. Additionally, a simple conditional-integration based anti-windup strategy
- Effective reference feedforward control

Future work

- descrete-time and real-time implementation;
- experimental validation in the laboratory;
- sensitivity and robustness analysis / consideration of parameter/model uncertainties; and
- avoidance of the need of matrix inversion (to avoid risk of numerical instability).

References I

[1] Christoph M. Hackl. A physics-based model of electro-active polymer actuators as the bases for a Gopinath-style motion state observer. Bachelorthesis, Lehrstuhl für Elektrische Antriebssysteme, Technische Universität München, Germany & Department of Mechanical Engineering and Department of Electrical & Computer Engineering, University of Wisconsin-Madison, USA, 2003.

[2] Christoph Hackl, H.-Y. Tang, R.D. Lorenz, L.-S. Turng, and Dierk Schröder. A multiphysics model of planar electro-active polymer actuators. In *Conference Record of the 39th IEEE Industrial Application Society Annual Meeting*, volume 3, pages 2125–2130. Institute of Electrical and Electronics Engineers (IEEE), 2004.

[3] Christoph Hackl, H.-Y. Tang, R.D. Lorenz, L.-S. Turng, and Dierk Schröder. A multidomain model of planar electro-active polymer actuators. *IEEE Transactions on Industry Applications*, 41(5):1142–1148, sep 2005.

[4] Christoph M. Hackl and Beatrix Mair. Optimale Bahnzugregelung am Beispiel einer Papierstreichanlage. In *Konferenzband des 9. Bahnlaufseminar*, TU Chemnitz, Deutschland, 2007.

[5] Christoph M. Hackl and Beatrix Mair. Optimierung der Bahnspannungsregelung durch dezentrale Regelsysteme auf der Basis von moderner Mikroelektronik und intelligenter Software zur Steigerung der Produktionssicherheit und der Produktivität von Papierstreichanlagen. Abschlussbericht zum Forschungsvorhaben AiF/IGF 14140N, Arbeitsgemeinschaft industrieller Forschungsvereinigungen “Otto von Guerick” (AiF), 2007.

[6] Beatrix Mair and Christoph M. Hackl. Optimierung der Bahnspannungsregelung durch dezentrale Regelsysteme auf der Basis von moderner Mikroelektronik und intelligenter Software zur Steigerung der Produktionssicherheit und der Produktivität von Papierstreichanlagen. PTS Forschungsbericht, The Paper Technology Specialists, Hessstr. 134, 80797 München, Germany, 2007.

[7] Christoph M. Hackl and Beatrix Mair. Besser Bahnen ziehen – Optimale Bahnzugregelung mit dSPACE-Prototyping-System. *dSPACE Magazine*, 2:40–45, 2008.

[8] Christoph M. Hackl and Beatrix Mair. Smoothing the tension - optimal web tension control with a dSPACE prototyping system. *dSPACE Magazine*, 2:40–45, 2008.

[9] Christian Endisch, Christoph Hackl, and Dierk Schröder. Optimal brain surgeon for general dynamic neural networks. In José Neves, Manuel Filipe Santos, and José Manuel Machado, editors, *Progress in Artificial Intelligence*, volume 4974/2007 of *Lecture Notes in Artificial Intelligence*, pages 15–28. Springer-Verlag, Berlin, 2007.

References II

[10] Christian Endisch, Christoph Hackl, and Dierk Schröder. System identification with general dynamic neural networks and network pruning. *International Journal of Computational Intelligence*, 4(3):187–195, 2007.

[11] Christian. Endisch, Peter Stolze, Peter Endisch, Christoph M.. Hackl, and Ralph M. Kennel. Levenberg-Marquardt-based OBS algorithm using adaptive pruning interval for system identification with dynamic neural networks. In *Proceedings of the IEEE International Conference on Systems, Man and Cybernetics*, pages 3402–3408, San Antonio, TX, USA, oct 2009. Institute of Electrical and Electronics Engineers (IEEE).

[12] C. Endisch, P. Stolze, C. Hackl, and D. Schröder. Comments on “Backpropagation algorithms for a broad class of dynamic networks”. *IEEE Transactions on Neural Networks*, 20(3):540–541, mar 2009.

[13] Mohamed Abdelrahem, Christoph Hackl, and Ralph Kennel. Application of extended kalman filter to parameter estimation of doubly-fed induction generators in variable-speed wind turbine systems. In *2015 International Conference on Clean Electrical Power (ICCEP)*. IEEE.

[14] Christoph M. Hackl. Speed funnel control with disturbance observer for wind turbine systems with elastic shaft. In *Proceedings of the 54th IEEE Conference on Decision and Control (CDC 2015)*, pages 2005–2012, Osaka, Japan, 2015.

[15] Simon Krüner and Christoph M. Hackl. Experimental identification of the optimal current vectors for a permanent-magnet synchronous machine in wave energy converters. *Energies*, 12(862), 2019.

[16] Christoph M. Hackl and Markus Landerer. A unified method for online detection of phase variables and symmetrical components of unbalanced three-phase systems with harmonic distortion. *Energies*, 12(17), 2019.

[17] Mohamed Abdelrahem, Ralph Kennel, Christoph Hackl, Mehmet Dal, and José Rodríguez. Efficient finite-position-set mras observer for encoder-less control of dfigs. In *2019 IEEE International Symposium on Predictive Control of Electrical Drives and Power Electronics (PRECEDE)*, pages 1–6, May 2019.

[18] Christoph M. Hackl and Markus Landerer. A unified method for generic signal parameter estimation of arbitrarily distorted single-phase grids with dc-offset. *IEEE Open Journal of the Industrial Electronics Society*, 1:235–246, 2020.

References III

[19] T. Kreppel, F. Rojas, C. M. Hackl, O. Kalmbach, M. Díaz, and G. Gatica. Extended Model of Chopper Cells for Open Circuit Fault Detection in Modular Multilevel Cascade Converters using Sliding Mode Observers. In *2020 IEEE 11th International Symposium on Power Electronics for Distributed Generation Systems (PEDG)*, pages 487–493, 2020. ISSN: 2329-5767.

[20] Mostafa Ahmed, Mohamed Abdelrahem, Ralph Kennel, and Christoph M. Hackl. A robust maximum power point tracking based model predictive control and extended kalman filter for pv systems. In *2020 International Symposium on Power Electronics, Electrical Drives, Automation and Motion (SPEEDAM)*, pages 514–519, 2020.

[21] Mostafa Ahmed, Mohamed Abdelrahem, Ralph Kennel, and Christoph M. Hackl. Maximum power point tracking based model predictive control and extended kalman filter using single voltage sensor for pv systems. In *2020 IEEE 29th International Symposium on Industrial Electronics (ISIE)*, pages 1039–1044, 2020.

[22] Christoph M. Hackl and Markus Landerer. Modified second-order generalized integrators with modified frequency locked loop for fast harmonics estimation of distorted single-phase signals. *IEEE Transactions on Power Electronics*, 2020.

[23] Julian Kullick and Christoph M Hackl. Nonlinear modeling, identification and optimal feedforward torque control of induction machines using steady-state machine maps. *IEEE Transactions on Industrial Electronics*, pages 1–1, 2022.

[24] Max A. Buettner, Niklas Monzen, and Christoph M. Hackl. Artificial neural network based optimal feedforward torque control of interior permanent magnet synchronous machines: A feasibility study and comparison with the state-of-the-art. *Energies*, 15(5):1838, 2022.

[25] Shih-Wei Su, Christoph M. Hackl, and Ralph Kennel. Analytical prototype functions for flux linkage approximation in synchronous machines. *IEEE Open Journal of the Industrial Electronics Society*, 3:265–282, 2022.

[26] Shih-Wei Su, Hannes Börngen, Christoph M. Hackl, and Ralph Kennel. Nonlinear current control of reluctance synchronous machines with analytical flux linkage prototype functions. *IEEE Open Journal of the Industrial Electronics Society*, pages 1–12, 2022.

[27] Christoph M. Hackl. *Contributions to High-gain Adaptive Control in Mechatronics*. PhD thesis, Lehrstuhl für Elektrische Antriebssysteme und Leistungselektronik, Technische Universität München (TUM), Germany, 2012.

References IV

[28] Christoph M. Hackl. Dynamische Reibungsmodellierung: Das Lund-Grenoble (LuGre) Reibmodell. In Dierk Schröder, editor, *Elektrische Antriebe – Regelung von Antriebssystemen*, chapter 25, pages 1615–1657. Springer-Verlag, 2015.

[29] Christoph M. Hackl. Dynamische Reibungsmodellierung: Das Lund-Grenoble (LuGre) Reibmodell. In Dierk Schröder, editor, *Elektrische Antriebe – Regelung von Antriebssystemen*, chapter 9.4, pages 1315–1357. Springer-Verlag, 2020.

[30] Hans Schuster, Christoph Michael Hackl, Christian Westermaier, and Dierk Schröder. Funnel-control for electrical drives with uncertain parameters. In *Proceedings of the 7th International Power Engineering Conference*, Singapore, 2005.

[31] Christoph M. Hackl and Dierk Schröder. Extension of high-gain controllable systems for improved accuracy. In *Proceedings of the 2006 IEEE International Conference on Control Applications (CCA 2006)*, pages 2231–2236, Munich, Germany, oct 2006. Institute of Electrical and Electronics Engineers (IEEE).

[32] Christoph Michael Hackl and Dierk Schröder. Funnel-control for nonlinear multi-mass flexible systems. In *Proceedings of the 32nd Annual Conference on IEEE Industrial Electronics*, pages 4707–4712, Paris, France, 2006.

[33] Christoph M. Hackl, Hans Schuster, Christian Westermaier, and Dierk Schröder. Funnel-control with integrating prefilter for nonlinear, time-varying two-mass flexible servo systems. In *Proceedings of the 9th International Workshop on Advanced Motion Control*, pages 456–461, Istanbul, Turkey, 2006. Institute of Electrical and Electronics Engineers (IEEE).

[34] Christoph M. Hackl, Yang Ji, and Dierk Schröder. Enhanced funnel-control with improved performance. In *Proceedings of the 15th Mediterranean Conference on Control and Automation*, pages Paper T01–016, Athens, Greece, jun 2007. Institute of Electrical and Electronics Engineers (IEEE).

[35] Christoph M. Hackl, Yang Ji, and Dierk Schröder. Funnel-control with constrained control input compensation. In *Proceedings of the 9th IASTED International Conference CONTROL AND APPLICATIONS*, pages 147–152, Montreal, Quebec, Canada, 2007.

[36] Christoph M. Hackl, Yang Ji, and Dierk Schröder. Nonidentifier-based adaptive control with saturated control input compensation. In *Proceedings of the 15th Mediterranean Conference on Control and Automation*, pages Paper T01–15, Athens, Greece, jun 2007. Institute of Electrical and Electronics Engineers (IEEE).

References V

[37] Christoph M. Hackl and Dierk Schröder. Funnel-control with online foresight. In *Proceedings of the 26th IASTED International Conference MODELLING, IDENTIFICATION AND CONTROL*, pages 171–176, Innsbruck, Austria, 2007.

[38] Christoph M. Hackl and Dierk Schröder. Non-identifier based adaptive control in robotics: An introduction. *International Journal of Factory Automation, Robotics and Soft Computing*, 4:90–99, 2008.

[39] Christoph M. Hackl, Christian Endisch, and Dierk Schröder. Specially designed funnel-control in mechatronics. In *Proceedings of the 5th International Conference on Computational Intelligence, Robotics and Autonomous Systems*, pages 59–64, 2008.

[40] Christoph M. Hackl, Christian Endisch, and Dierk Schröder. Contributions to non-identifier based adaptive control in mechatronics. *Robotics and Autonomous Systems, Elsevier*, 57(10):996–1005, 2009.

[41] Christoph M. Hackl. Funnel Control: Implementierung, Erweiterung und Anwendung. In Dierk Schröder, editor, *Intelligente Verfahren: Systemidentifikation und Regelung nichtlinearer Systeme*, pages 697–760. Springer-Verlag, Berlin, 2010.

[42] Christoph M. Hackl and Stephan Trenn. The bang-bang funnel controller: An experimental verification. *PAMM*, 12(1):735–736, dec 2012.

[43] Christoph M. Hackl, Norman Hopfe, Achim Ilchmann, Markus Mueller, and Stephan Trenn. Funnel control for systems with relative degree two. *SIAM Journal on Control and Optimization*, 51(2):965–995, jan 2013.

[44] Christoph M. Hackl. Funnel control for wind turbine systems. In *Proceedings of the 2014 IEEE International Conference on Control Applications (CCA 2014)*, pages 1377–1382, Antibes, France, oct 2014. Institute of Electrical and Electronics Engineers (IEEE).

[45] Christoph M. Hackl. Current PI-funnel control with anti-windup for synchronous machines. In *Proceedings of the 54th IEEE Conference on Decision and Control (CDC 2015)*, pages 1997–2004, Osaka, Japan, dec 2015. Institute of Electrical and Electronics Engineers (IEEE).

[46] Christoph M. Hackl. *Non-identifier based adaptive control in mechatronics: Theory and Application*. Number 466 in Lecture Notes in Control and Information Sciences. Springer International Publishing, Berlin, 2017.

[47] Christoph M. Hackl, Christian Endisch, and Dierk Schröder. Applicability of funnel-control in robotics. In *Proceedings of the 5th International Conference on Computational Intelligence, Robotics and Autonomous Systems*, pages 65–70, Linz, Austria, 2008.

References VI

[48] Christoph M. Hackl, Christian Endisch, and Dierk Schröder. Funnel-control in robotics: An introduction. In *Proceedings of the 16th Mediterranean Conference on Control and Automation*, pages 913–919, Ajaccio, France, jun 2008. Institute of Electrical and Electronics Engineers (IEEE).

[49] Christoph M. Hackl and Dierk Schröder. Non-identifier based adaptive control in robotics: An introduction. In Salvatore Pennacchio, editor, *Recent adavances in Control Systems, Robotics and Automation*, volume 1. INTERNATIONALSAR International Society for Advanced Research, Palermo, Italy, third edition, 2009.

[50] Christoph M. Hackl. High-gain adaptive position control. *International Journal of Control*, 84(10):1695–1716, oct 2011.

[51] Christoph M. Hackl, Andreas G. Hofmann, Rik W. De Doncker, and Ralph M. Kennel. Funnel control for speed & position control of electrical drives: A survey. In *Proceedings of the 19th Mediterranean Conference on Control & Automation (MED)*, pages 181–188, Corfu Island, Greece, jun 2011. Institute of Electrical and Electronics Engineers (IEEE).

[52] Christoph M. Hackl, Andreas G. Hofmann, and Ralph M. Kennel. Funnel control in mechatronics: An overview. In *Proceedings of the 50th IEEE Conference on Decision and Control (CDC) and European Control Conference (ECC)*, pages 8000–8007, Orlando, FL, USA, dec 2011. Institute of Electrical and Electronics Engineers (IEEE).

[53] Christoph M. Hackl. 'Funnel control' zur Positionsregelung von starren Drehgelenkrobotern mit grob bekannter Trägheitsmatrix. In *Tagungsband des GMA-Fachausschuss 1.40*, pages 302–310, Anif, Austria, 2012.

[54] Christoph M. Hackl and Ralph M. Kennel. Position funnel control for rigid revolute joint robotic manipulators with known inertia matrix. In *Proceedings of the 20th Mediterranean Conference on Control and Automation*, pages 615–620, Barcelona, Spain, jul 2012. Institute of Electrical and Electronics Engineers (IEEE).

[55] Christoph M. Hackl and Ralph M. Kennel. Position funnel control with linear internal model. In *Proceedings of 2012 IEEE International Conference on Control Applications (CCA 2012)*, pages 1334–1339, Dubrovnik, Croatia, oct 2012. Institute of Electrical and Electronics Engineers (IEEE).

[56] Timm Faulwasser and Christoph M. Hackl. Path-following funnel control for rigid-link revolute-joint robotic systems. In *Proceedings of the 21st International Symposium on Mathematical Theory of Networks and Systems*, pages 1044–1051, Groningen, Netherlands, 2014.

References VII

[57] Julian Kullick and Christoph Hackl. Dynamic Modeling and Simulation of Deep Geothermal Electric Submersible Pumping Systems. *Energies*, 10(10):1659, October 2017.

[58] Florian Bauer, Christoph M. Hackl, Keyue Ma Smedley, and Ralph M. Kennel. Multicopter with series connected propeller drives. *IEEE Transactions on Control Systems Technology*, pages 1–12, 2017.

[59] Christoph M. Hackl, Florian Larcher, Alexander Dötlinger, and Ralph. M. Kennel. Is multiple-objective model-predictive control "optimal"? In *Proceedings of the 2013 IEEE International Symposium on Predictive Control of Electrical Drives and Power Electronics (PRECEDE 2013)*, pages 1–8, Munich, Germany, oct 2013. Institute of Electrical and Electronics Engineers (IEEE).

[60] Z. Zhang, C. Hackl, F. Wang, Z. Chen, and R. Kennel. Encoderless model predictive control of back-to-back converter direct-drive permanent-magnet synchronous generator wind turbine systems. In *Proceedings of 15th European Conference on Power Electronics and Applications*, pages 1–10. Institute of Electrical and Electronics Engineers (IEEE), sep 2013.

[61] Mohamed Abdelrahem, Christoph M. Hackl, and Ralph Kennel. Sensorless control of doubly-fed induction generators in variable-speed wind turbine systems. In *Proceedings of the 5th International Conference on Clean Electrical Power (ICCEP)*, pages 423–430, Taormina, Italy, jun 2015. Institute of Electrical and Electronics Engineers (IEEE).

[62] Christian Dirscherl, Josef Fessler, Christoph Hackl, and Hanko Ipach. State-feedback control and observer design of grid-connected power inverters with LCL-filter. In *Proceedings of the 5th Colloquium of the Munich School of Engineering*, Garching, Germany, 2015.

[63] Christian Dirscherl, Josef Fessler, Christoph M. Hackl, and Hanko Ipach. State-feedback controller and observer design for grid-connected voltage source power converters with LCL-filter. In *Proceedings of the 2015 IEEE International Conference on Control Applications (CCA 2015)*, pages 215–222, Sydney, Australia, sep 2015. Institute of Electrical and Electronics Engineers (IEEE).

[64] Christian Dirscherl, Christoph Hackl, and Korbinian Schechner. Explicit model predictive control with disturbance observer for grid-connected voltage source power converters. In *Proceedings of the 2015 IEEE International Conference on Industrial Technology (ICIT 2015)*, pages 999–1006. Institute of Electrical and Electronics Engineers (IEEE), mar 2015.

References VIII

[65] Christian Dirscherl, Christoph M. Hackl, and Korbinian Schechner. Pole-placement based nonlinear state-feedback control of the DC-link voltage in grid-connected voltage source power converters: A preliminary study. In *Proceedings of the 2015 IEEE International Conference on Control Applications (CCA 2015)*, pages 207–214, Sydney, Australia, sep 2015. Institute of Electrical and Electronics Engineers (IEEE).

[66] Christoph M. Hackl. MPC with analytical solution and integral error feedback for LTI MIMO systems and its application to current control of grid-connected power converters with LCL-filter. In *Proceedings of the 2015 IEEE International Symposium on Predictive Control of Electrical Drives and Power Electronics (PRECEDE 2015)*, pages 61–66, Valparaiso, Chile, oct 2015. Institute of Electrical and Electronics Engineers (IEEE).

[67] Zhenbin Zhang, Hue Xu, M. Xue, Z. Chen, T. Sun, Ralph Kennel, and Christoph Hackl. Predictive control with novel virtual flux estimation for back-to-back power converters. *IEEE Transactions on Industrial Electronics*, 62(5):2823–2834, may 2015.

[68] Ayman Ayad, Mohamed Hashem, Christoph Hackl, and Ralph Kennel. Proportional-resonant controller design for quasi-Z-source inverters with LC filters. In *Proceedings of the 42nd IEEE Industrial Electronics Conference (IECON 2016)*, Firenze, Italy, 2016.

[69] Christoph M. Hackl. On the equivalence of proportional-integral and proportional-resonant controllers with anti-windup. *arXiv:1610.07133*, 2016.

[70] Josh C. Mitchell, Maarten J. Kamper, and Christoph M. Hackl. Small-scale reluctance synchronous generator variable speed wind turbine system with DC transmission linked inverters. In *Proceedings of the IEEE Energy Conversion Congress & Exposition (ECCE)*, Milwaukee, WI, USA, 2016.

[71] Zhenbin Zhang, Christoph Hackl, Mohamed Abdelrahem, and Ralph Kennel. Voltage sensorless direct model predictive control of 3L-NPC back-to-back power converter PMSG wind turbine systems with fast dynamics. In *Proceedings of the Power Electronics Student Summit (PESS 2016)*, Aachen, Germany, 2016.

[72] Zhenbin Zhang, Christoph Hackl, and Ralph Kennel. Computationally efficient DMPC for three-level NPC back-to-back converters in wind turbine systems with PMSG. *IEEE Transactions on Power Electronics*, 32:8018–8034, 2017.

[73] Zhenbin Zhang, Christoph Hackl, and Ralph Kennel. FPGA based direct model predictive current control of PMSM drives with 3L-NPC power converters. In *Proceedings of the PCIM Europe 2016*, 2016.

References IX

[74] Zhenbin Zhang, Ralph Kennel, and Christoph Hackl. Computationally efficient direct model predictive control for three-level NPC back-to-back converter PMSG wind turbine systems. In *Proceedings of the 2016 International Symposium on Power Electronics, Electrical Drives, Automation and Motion (SPEEDAM 2016)*, pages 1045–1050, Anacapri, Italy, jun 2016. Institute of Electrical and Electronics Engineers (IEEE).

[75] Zhenbin Zhang, Ralph Kennel, and Christoph M. Hackl. Performance-enhanced direct multiple-vector model predictive power control for grid-tied AFEs. In *Proceedings of the 2016 IEEE 8th International Power Electronics and Motion Control Conference (IPEMC-ECCE Asia)*, pages 2904–2909, Hefei, China, may 2016. Institute of Electrical and Electronics Engineers (IEEE).

[76] Mohamed Abdelrahem, Christoph Michael Hackl, and Ralph Kennel. Finite set model predictive control with on-line parameter estimation for active frond-end converters. *Electrical Engineering*, 100(3):1497–1507, Sep 2018.

[77] M. Espinoza, R. Cardenas, J. C. Clare, D. Soto, M. Diaz, E. Espina, and C. M. Hackl. An integrated converter and machine control system for mmc-based high power drives. *IEEE Transactions on Industrial Electronics*, PP(99):1–1, 2018.

[78] Christoph M. Hackl, Urs Pecha, and Korbinian Schechner. Modeling and control of permanent-magnet synchronous generators under open-switch converter faults. *IEEE Transactions on Power Electronics*, 2018.

[79] Korbinian Schechner, Florian Bauer, and Christoph M. Hackl. Nonlinear DC-link PI control for airborne wind energy systems during pumping mode. In Roland Schmehl, editor, *Airborne Wind Energy: Advances in Technology Development and Research*. Springer Singapore, 2019.

[80] M. Diaz, R. Cardenas, M. Espinoza, C. M. Hackl, F. Rojas, J. C. Clare, and P. Wheeler. Vector control of a modular multilevel matrix converter operating in the full output-frequency range. *IEEE Transactions on Industrial Electronics*, 66(7):5102–5114, July 2019.

[81] Michael Saegmueller, Christoph Hackl, Rolf Witzmann, and Rene Richter. Analytic solutions for minimum conduction loss modulation of dual active bridge converters including frequency variation. In *IECON 2020 The 46th Annual Conference of the IEEE Industrial Electronics Society*. IEEE, oct 2020.

[82] O. Kalmbach, C. M. Hackl, and F. Rojas. A Generic Switching State-Space Model for Modular Multilevel Cascade Converters. In *2020 IEEE 11th International Symposium on Power Electronics for Distributed Generation Systems (PEDG)*, pages 447–454, 2020.

References X

[83] Oliver Kalmbach, Christian Dirscherl, and Christoph M. Hackl. Discrete-Time DC-Link Voltage and Current Control of a Grid-Connected Inverter with LCL-Filter and Very Small DC-Link Capacitance. *Energies*, 13(21):5613, 2020.

[84] Mostafa Ahmed, Mohamed Abdelrahem, Ralph Kennel, and Christoph M. Hackl. An enhanced maximum power point tracking based finite-control-set model predictive control for pv systems. In *2020 11th Power Electronics, Drive Systems, and Technologies Conference (PEDSTC)*, pages 1–6, 2020.

[85] Christoph Hackl, Christian Dirscherl, and Korbinian Schechner. Modellierung und Regelung von Windkraftanlagen (see https://arxiv.org/abs/1703.08661 for the english translation). In Dierk Schröder, editor, *Elektrische Antriebe – Regelung von Antriebssystemen*, chapter 10.3, pages 1504–1585. Springer-Verlag, 2020.

[86] Michael Saegmueller, Christoph Hackl, Rolf Witzmann, and René Richter. Analytic solutions for full operating range single-side zvs modulation of dual active bridge converters. In *Proceedings of the IEEE International Symposium on Industrial Electronics (ISIE) 2021*. IEEE, 2021.

[87] Christoph Hackl, Simon Krüner, and Zhao Song. 3d-modulation and pi state-feedback control for voltage source inverters with split dc-link. In *Proceedings of the IEEE International Symposium on Industrial Electronics (ISIE) 2021*. IEEE, 2021.

[88] Ibrahim Harbi, Mostafa Ahmed, Christoph M. Hackl, Ralph Kennel, and Mohamed Abdelrahem. A nine-level split-capacitor active-neutral-point-clamped inverter and its optimal modulation technique. *IEEE Transactions on Power Electronics*, 37(7):8045–8064, 2022.

[89] Christoph M. Hackl, Christian Endisch, and Dierk Schröder. Error reference control of nonlinear two-mass flexible servo systems. In *Proceedings of the 16th Mediterranean Conference on Control and Automation*, pages 1047–1053, Ajaccio, France, jun 2008. Institute of Electrical and Electronics Engineers (IEEE).

[90] Peter Landsmann, Christoph M. Hackl, and Ralph M. Kennel. Eliminating all machine parameters in encodersless predictive torque control without signal injection. In *Proceedings of the 2011 IEEE International Electric Machines and Drives Conference*, pages 1259–1264. Institute of Electrical and Electronics Engineers (IEEE), may 2011.

References XI

[91] Christoph M. Hackl. Funnel control with disturbance observer for two-mass systems. In *Proceedings of the 52nd IEEE Conference on Decision and Control (CDC)*, pages 6244–6249, Florence, Italy, dec 2013. Institute of Electrical and Electronics Engineers (IEEE).

[92] Christoph M. Hackl. PI-funnel control with Anti-windup and its application for speed control of electrical drives. In *Proceedings of the 52nd IEEE Conference on Decision and Control (CDC)*, pages 6250–6255, Florence, Italy, dec 2013. Institute of Electrical and Electronics Engineers (IEEE).

[93] Christian Dirscherl, Christoph M. Hackl, and Korbinian Schechner. Modeling and control of wind turbine systems with permanent-magnet synchronous generators (PMSG) and doubly fed induction generators (DFIG). In *Proceedings of the 4th Colloquium of the Munich School of Engineering*, Garching, Germany, 2014.

[94] Christoph M. Hackl. Klein-Windkraftanlagen mit effizienter und kostengünstiger Generatortopologie für Micro-Grids: Eine Voruntersuchung. In *Poster auf der Jahresversammlung des Bundes der Freunde der Technischen Universität München e.V.*, Munich, Germany, 2014.

[95] Christoph Hackl and Korbinian Schechner. Non-ideal torque control in wind turbine systems: Causes and impacts. In *Proceedings of the 5th Colloquium of the Munich School of Engineering*, Garching, Germany, 2015.

[96] Christoph M. Hackl, Maarten J. Kamper, Julian Kullick, and Joshua Mitchell. Nonlinear PI current control of reluctance synchronous machines. 2015.

[97] Christoph M. Hackl and Korbinian Schechner. Non-ideal torque control in wind turbine systems: Causes and impacts. In *Proceedings of the $5^{\rm th}$ MSE-Kolloquium on "Innovations for Energy Systems, Mobility, Buildings and Materials"*, Munich, Germany, 2015.

[98] Mohamed Abdelrahem, Christoph M. Hackl, and Ralph Kennel. Encoderless model predictive control of doubly-fed induction generators in variable-speed wind turbine systems. In *Proceedings of the 6th edition of the conference "The Science of Making Torque from Wind" (TORQUE 2016)*, Open access Journal of Physics: Conference Series 753 (2016) 112005, Munich, Germany, 2016.

References XII

[99] Hisham Eldeeb, Christoph M. Hackl, Lorenz Horlbeck, and Julian Kullick. On the optimal feedforward torque control problem of anisotropic synchronous machines: Quadrics, quartics and analytical solutions. 2016.

[100] Hisham Eldeeb, Christoph M. Hackl, and Julian Kullick. Efficient operation of anisotropic synchronous machines for wind energy systems. In *Proceedings of the 6th edition of the conference "The Science of Making Torque from Wind" (TORQUE 2016)*, Open access Journal of Physics: Conference Series 753 (2016) 112005, Munich, Germany, 2016.

[101] Christoph M. Hackl, Maarten J. Kamper, Julian Kullick, and Joshua Mitchell. Current control of reluctance synchronous machines with online adjustment of the controller parameters. In *Proceedings of the 2016 IEEE International Symposium on Industrial Electronics (ISIE 2016)*, pages 153–160. Institute of Electrical and Electronics Engineers (IEEE).

[102] Lorenz Horlbeck and Christoph M. Hackl. Analytical solution for the MTPV hyperbola including the stator resistance. In *Proceedings of the IEEE International Conference on Industrial Technology (ICIT 2016)*, pages 1060–1067, Taipei, Taiwan, mar 2016. Institute of Electrical and Electronics Engineers (IEEE).

[103] Zhenbin Zhang, Ralph Kennel, and Christoph M. Hackl. Two direct torque and power control methods for back-to-back power converter PMSG wind turbine systems. In *Proceedings of the 2016 IEEE 8th International Power Electronics and Motion Control Conference (IPEMC-ECCE Asia)*, pages 1515–1520, Hefei, China, may 2016. Institute of Electrical and Electronics Engineers (IEEE).

[104] Mohamed. Abdelrahem, Christoph Hackl, and Ralph Kennel. Finite Position Set-Phase Locked Loop for Sensorless Control of Direct-Driven Permanent-Magnet Synchronous Generators. *IEEE Transactions on Power Electronics*, PP(99):1–1, 2017.

[105] Hisham Eldeeb, Christoph M. Hackl, Lorenz Horlbeck, and Julian Kullick. A unified theory for optimal feedforward torque control of anisotropic synchronous machines. *International Journal of Control*, 2017.

[106] Hisham Eldeeb, Christoph M. Hackl, Lorenz Horlbeck, and Julian Kullick. Analytical solutions for the optimal reference currents for MTPC/MTPA, MTPV and MTPF control of anisotropic synchronous machines. In *Proceedings of the IEEE International Electric Machines & Drives Conference (IEMDC 2017)*, pages 1–6, Miami, FL, USA, 2017.

[107] Mohamed Abdelrahem, Christoph Michael Hackl, and Ralph Kennel. Implementation and experimental investigation of a sensorless field-oriented control scheme for permanent-magnet synchronous generators. *Electrical Engineering*, may 2017.

References XIII

[108] A. D. Birda, J. Reuss, and C. Hackl. Synchronous optimal pulse-width modulation with differently modulated waveform symmetry properties for feeding synchronous motor with high magnetic anisotropy. In *2017 19th European Conference on Power Electronics and Applications (EPE'17 ECCE Europe)*, pages P.1–P.10, Sept 2017.

[109] H. Eldeeb, C. Hackl, M. Abdelrahem, and A. S. Abdel-Khalik. A unified SVPWM realization for minimizing circulating currents of dual three phase machines. In *2017 IEEE 12th International Conference on Power Electronics and Drive Systems (PEDS)*, pages 925–931, Dec 2017.

[110] Mauricio Espinoza, Matias Díaz, Enrique Espina, Christoph M. Hackl, and Roberto Cardénas. Control strategies for modular multilevel converters driving cage machines. In *Proceedings of the 3rd IEEE Southern Power Electronics Conference (SPEC 2017)*, pages 1–6, Dec 2017.

[111] Mohamed Abdelrahem, Christoph M. Hackl, Zhenbin Zhang, and Ralph Kennel. Robust predictive control for direct-driven surface-mounted permanent-magnet synchronous generators without mechanical sensors. *IEEE Transactions on Energy Conversion*, 33(1):179–189, 2018.

[112] Korbinian Schechner and Christoph M. Hackl. Scaling of the drive train dynamics of large-scale wind turbine systems for real-time emulation in small-scale laboratory setups. *IEEE Transactions on Industrial Electronics*, 66(9):6779–6788, 2018.

[113] H. Eldeeb, A. S. Abdel-Khalik, and C. Hackl. Dynamic modelling of dual three-phase IPMSM drives with different neutral configurations. *IEEE Transactions on Industrial Electronics*, PP(99):1–1, 2018.

[114] H. Eldeeb, M. Abdelrahem, C. Hackl, and A. S. Abdel-Khalik. Enhanced electromechanical modeling of asymmetrical dual three-phase IPMSM drives. In *2018 IEEE 27th International Symposium on Industrial Electronics (ISIE)*, pages 126–132, June 2018.

[115] H. Eldeeb, A. S. Abdel-Khalik, and C. Hackl. Post-fault full torque-speed exploitation of dual three-phase IPMSM drives. *IEEE Transactions on Industrial Electronics*, 2018.

[116] Hisham Magdy Eldeeb, Ayman Samy Abdel-Khalik, Julian Kullick, and Christoph M. Hackl. Pre and post-fault current control of dual three-phase reluctance synchronous drives. *IEEE Transactions on Industrial Electronics*, pages 1–1, 2019.

References XIV

[117] Athina Birda, Jörg Reuss, and Christoph M. Hackl. Simple fundamental current estimation and smooth transition between synchronous optimal pwm and asynchronous svm. *IEEE Transactions on Industrial Electronics*, pages 1–1, 2019.

[118] Xiaonan Gao, Mohamed Abdelrahem, Christoph M. Hackl, Zhenbin Zhang, and Ralph Kennel. Direct predictive speed control with a sliding manifold term for pmsm drives. *IEEE Journal of Emerging and Selected Topics in Power Electronics*, pages 1–1, 2019.

[119] Mohamed Abdelrahem, Christoph Michael Hackl, Ralph Kennel, and José Rodríguez. Efficient direct-model predictive control with discrete-time integral action for pmsgs. *IEEE Transactions on Energy Conversion*, 34(2):1063–1072, 2019.

[120] Mohamed Abdelrahem, Christoph Hackl, Ralph Kennel, and Jose Rodriguez. Sensorless predictive speed control of permanent-magnet synchronous generators in wind turbine applications. In *PCIM Europe 2019; International Exhibition and Conference for Power Electronics, Intelligent Motion, Renewable Energy and Energy Management*, pages 1–8, May 2019.

[121] Shih-Wei Su, Ralph Kennel, and Christoph M. Hackl. Analytical flux linkage approximation prototypes for reluctance synchronous machines. In *2020 International Symposium on Power Electronics, Electrical Drives, Automation and Motion (SPEEDAM)*. IEEE, jun 2020.

[122] Mohamed Abdelrahem, Christoph M. Hackl, José Rodríguez, and Ralph Kennel. Model reference adaptive system with finite-set for encoderless control of PMSGs in micro-grid systems. *Energies*, 13(18):4844, sep 2020.

[123] Christoph Hackl, Julian Kullick, and Niklas Monzen. Optimale Betriebsführung für nichtlineare Synchronmaschinen. In Joachim Böcker and Gerd Griepentrog, editors, *Elektrische Antriebe – Regelung von Antriebssystemen*. Springer-Verlag, 2020.

[124] Antonin Glac, Vaclav Smidl, Zdenek Peroutka, and Christoph M. Hackl. Comparison of IPMSM parameter estimation methods for motor efficiency. In *IECON 2020 The 46th Annual Conference of the IEEE Industrial Electronics Society*. IEEE, oct 2020.

[125] Christoph Hackl, Julian Kullick, and Peter Landsmann. Nichtlineare Stromregelverfahren für Reluktanz-Synchronmaschinen. In Joachim Böcker and Gerd Griepentrog, editors, *Elektrische Antriebe – Regelung von Antriebssystemen*. Springer-Verlag, 2020.

[126] Ahmed Farhan, Mohamed Abdelrahem, Christoph M. Hackl, Ralph Kennel, Adel Shaltout, and Amr Saleh. Advanced strategy of speed predictive control for nonlinear synchronous reluctance motors. *Machines*, 8(3):44, aug 2020.

References XV

[127] Mohamed Abdelrahem, Christoph Hackl, Ralph Kennel, and Jose Rodriguez. Low sensitivity predictive control for doubly-fed induction generators based wind turbine applications. *Sustainability*, 13(16):9150.

[128] Athina Birda, Joerg Reuss, and Christoph M. Hackl. Synchronous optimal pulsewidth modulation for synchronous machines with highly operating point dependent magnetic anisotropy. *IEEE Transactions on Industrial Electronics*, 68(5):3760–3769, may 2021.

[129] Athina Birda, Christoph Grabher, Joerg Reuss, and Christoph M. Hackl. Dc-link capacitor and inverter current ripples in anisotropic synchronous motor drives produced by synchronous optimal pwm. *IEEE Transactions on Industrial Electronics*, jan 2021.

[130] Andrea Zanelli, Julian Kullick, Hisham Eldeeb, Gianluca Frison, Christoph Hackl, and Moritz Diehl. Continuous control set nonlinear model predictive control of reluctance synchronous machines. *IEEE Transactions on Control Systems Technology*, pages 1–12, 2021.

[131] C. M. Hackl, J. Kullick, and N. Monzen. Generic loss minimization for nonlinear synchronous machines by analytical computation of optimal reference currents considering copper and iron losses. In *2021 IEEE International Conference on Industrial Technology (ICIT)*. IEEE, mar 2021.

[132] Mohamed Abdelrahem, Christoph M. Hackl, Ralph Kennel, and Jose Rodriguez. Computationally efficient finite-position-set-phase-locked loop for sensorless control of PMSGs in wind turbine applications. *IEEE Transactions on Power Electronics*, 36(3):3007–3016, mar 2021.

[133] Antonín Glac, Václav Šmídl, Zdeněk Peroutka, and Christoph M. Hackl. Dependence of IPMSM motor efficiency on parameter estimates. *Sustainability*, 13(16):9299.

[134] Haotian Xie, Jianming Du, Dongliang Ke, Yingjie He, Fengxiang Wang, Christoph Hackl, José Rodríguez, and Ralph Kennel. Multistep model predictive control for electrical drives—a fast quadratic programming solution. *Symmetry*, 14(3):626.

[135] Issa Hammoud, Sebastian Hentzelt, Ke Xu, Thimo Oehlschlaegel, Mohamed Abdelrahem, Christoph M. Hackl, and Ralph Kennel. On continuous set model predictive control of permanent magnet synchronous machines. *IEEE Transactions on Power Electronics*, pages 1–1, 2022.

References XVI

[136] Julian Kullick and Christoph M. Hackl. Speed-sensorless control of induction machines with LC filter for geothermal electric submersible pumping systems. *Machines*, 10(2):87.

[137] Yuebin Pang, Jovan Knezevic, Daniel Glose, and Christoph Hackl. Sensorless control of electrically excited synchronous machines considering magnetic saturation and flux linkage dynamics for automotive applications. *IEEE Transactions on Industrial Electronics*, pages 1–11.

[138] Simon Wiedemann and Christoph M. Hackl. Simultaneous identification of inverter and machine nonlinearities for self-commissioning of electrical synchronous machine drives. *IEEE Transactions on Energy Conversion*, pages 1–14, 2023.

[139] Johannes Rossmann, Maarten J. Kamper, and Christoph M. Hackl. Single-objective machine design with gaussian process regression and bayesian optimization (extended version). *techrxiv.org (preprint)*, May 2024.

[140] Johannes Rossmann, Maarten J. Kamper, and Christoph M. Hackl. Multi-objective machine design optimization withgaussian process regression and bayesianoptimization (extended version). *techrxiv.org (preprint)*, May.

[141] Christian Dirscherl, Christoph Hackl, and Korbinian Schechner. Modellierung und Regelung von modernen Windkraftanlagen: Eine Einführung (see https://arxiv.org/abs/1703.08661 for the english translation). In Dierk Schröder, editor, *Elektrische Antriebe – Regelung von Antriebssystemen*, chapter 24, pages 1540–1614. Springer-Verlag, 2015.

[142] Florian Bauer, Christoph M. Hackl, and Korbinian Schechner. DC-link control for airborne wind energy systems during pumping mode. In *Proceedings of the Airborne Wind Energy Conference (AWEC 2015)*, Delft, Netherlands, 2015.

[143] Mohamed Abdelrahem, Christoph M. Hackl, and Ralph Kennel. Model predictive control of permanent magnet synchronous generators in variable-speed wind turbine systems. In *Proceedings of the Power Electronics Student Summit (PESS 2016)*, Aachen, Germany, 2016.

[144] Mohamed Abdelrahem, Christoph Michael Hackl, and Ralph Kennel. Simplified model predictive current control without mechanical sensors for variable-speed wind energy conversion systems. *Electrical Engineering*, 99(1):367–377, 2016.

References XVII

[145] Mohamed Abdelrahem, Christoph M. Hackl, Zhenbin Zhang, and Ralph Kennel. Sensorless control of permanent magnet synchronous generators in variable-speed wind turbine systems. In *Proceedings of the Power Electronics Student Summit (PESS 2016)*, Aachen, Germany, 2016.

[146] Florian Bauer, Christoph M. Hackl, K. Smedley, and Ralph Kennel. Virtual-power-hardware-in-the-loop simulations in crosswind kite power with ground generation. In *Proceedings of the 2016 American Control Conference (ACC)*, pages 4071–4076, Boston, FL, USA, jul 2016. Institute of Electrical and Electronics Engineers (IEEE).

[147] Christian Dirscherl and Christoph M. Hackl. Dynamic power flow in wind turbine systems with doubly-fed induction generator. In *Proceedings of the 2016 IEEE International Energy Conference (ENERGYCON 2016)*, pages 1–6, Leuven, Beglium, apr 2016. Institute of Electrical and Electronics Engineers (IEEE).

[148] Christoph M. Hackl and Korbinian Schechner. Non-ideal feedforward torque control of wind turbines: Impacts on annual energy production & gross earnings. In *Proceedings of the 6th edition of the conference "The Science of Making Torque from Wind" (TORQUE 2016)*, volume 753 of *Open access Journal of Physics: Conference Series 753 (2016) 112005*, page 112010, Munich, Germany, sep 2016. IOP Publishing.

[149] Florian Bauer, Ralph M. Kennel, Christoph M. Hackl, Filippo Campagnolo, Michael Patt, and Roland Schmehl. Drag power kite with very high lift coefficient. *Renewable Energy*, October 2017.

[150] Christian Dirscherl and Christoph M. Hackl. Local stability analysis and controller design for speed-controlled wind turbine systems in regime ii.5. *Energies*, (5):33, 2018.

[151] Christoph M. Hackl, Pol Jané-Soneira, Martin Pfeifer, Korbinian Schechner, and Sören Hohmann. Full- and reduced-order state-space modeling of wind turbine systems with permanent magnet synchronous generator. *Energies*, (7):33, 2018.

[152] S. Hanif, K. Zhang, C. Hackl, M. Barati, H. B. Gooi, and T. Hamacher. Decomposition and equilibrium achieving distribution locational marginal prices using trust-region method. *IEEE Transactions on Smart Grid*, PP(99):1–1, 2018.

[153] Mohamed Abdelrahem, Christoph Hackl, Ahmed Farhan, and Ralph Kennel. Finite-set mras observer for encoderless control of pmsgs in wind turbine applications. In *2019 IEEE Conference on Power Electronics and Renewable Energy (CPERE)*, pages 431–436, 2019.

References XVIII

[154] Katharina Bär, Abdessamad Saidi, Christoph Hackl, and Wilfried Zörner. Combined operation of photovoltaic and biogas plants for optimal transformer loading. *Chemical Engineering Transactions*, 76:601–606.

[155] Kai Zhang, Sarmad Hanif, Christoph M. Hackl, and Thomas Hamacher. A framework for multi-regional real-time pricing in distribution grids. *IEEE Transactions on Smart Grid*, 10(6):6826–6838, Nov 2019.

[156] Florian Bauer, Christoph M. Hackl, Keyue Smedley, and Ralph Kennel. Crosswind kite power with tower. In Roland Schmehl, editor, *Airborne Wind Energy: Advances in Technology Development and Research*. Springer-Verlag, 2019.

[157] Florian Bauer, Christoph M. Hackl, Keyue Smedley, and Ralph Kennel. On multicopter-based launching and landing of lift power kites. In Roland Schmehl, editor, *Airborne Wind Energy: Advances in Technology Development and Research*. Springer-Verlag, 2019.

[158] Mohamed Abdelrahem, Christoph Hackl, and Ralph Kennel. Robust predictive control scheme for permanent-magnet synchronous generators based modern wind turbines. *Electronics*, 10(13):1596.

[159] D. Schröder and C.M. Hackl. Grundlagen der Regelungstechnik. IHK Schwaben, Mechatronik Weiterbildung, 2009.

[160] Christoph Hackl. *Bewegungssteuerung durch geregelte elektrische Antriebe (Übung)*. Lehrstuhl für Elektrische Antriebe und Leistungselektronik – Technische Universität München, 2013.

[161] Christoph M. Hackl. Regelung von regenerativen Energiesystemen (Vorlesungsskriptum und Übungsaufgaben). online, 2014. Lehrmaterialien zur Veranstaltung "Regelung von regenerativen Energiesystemen" im Wintersemester 2013/2014 an der Technischen Universität München.

[162] Christoph M. Hackl. Projektstudium Antriebstechnik: Projektbezogen Studieren – Aktives Lernen im Team. online, 2015. Kurzskriptum mit Projektbeschreibungen zur Umsetzung des Ernst-Otto Fischer Lehrpreises 2013 im Wintersemester 2014/2015 an der Technischen Universität München.

[163] Christoph Hackl, Ellen Taraba, and Anne-Marie Fleischmann. Projektbezogen Studieren – Aktives Lernen im Team: Fachliche und überfachliche Kompetenzen von Studierenden fördern. In *Tagungsband des 2. HD-MINT-Symposium Hochschuldidaktik für MINT-Fächer*, Nürnberg, Germany, 2015.

References XIX

[164] Christoph M. Hackl, Anne-Marie Fleischmann, and Ellen Taraba. Projektstudium Antriebstechnik: Projektbezogen Studieren – Aktives Lernen im Team. In *Tagungsband des 5. VDI Qualitätsdialogs Lehre - Studienerfolg verbessern*, Tagungswerk Jerusalemkirche, Berlin, Germany, 2015.

[165] Christoph Hackl, Anne-Marie Lickert, and Ellen Taraba. Projektbezogen Studieren – Aktives Lernen im Team. In *Neues Handbuch Hochschullehre*, volume 76, pages 31–44. DUZ Medienhaus, 2016.

[166] Oliver Kalmbach and Christoph M. Hackl. Cluster-fault control strategies for modular multilevel converters. 6:685–707.

[167] Zhao Song, Simon Krüner, and Christoph M. Hackl. Modeling and proportional-integral state feedback control of fully parallel grid-connected inverters. 6:618–636.

[168] Niklas Monzen, Florian Stroebl, Herbert Palm, and Christoph M. Hackl. Multiobjective hyperparameter optimization of artificial neural networks for optimal feedforward torque control of synchronous machines. *IEEE Open Journal of the Industrial Electronics Society*, 5:41–53, 2024.

[169] Andre Thommessen and Christoph Michael Hackl. Virtual synchronous machine control for doubly fed induction machine-based wind energy conversion systems. *IEEE Open Journal of the Industrial Electronics Society*, 5:264–301, 2024.

[170] Christoph Goettsberger and Christoph M. Hackl. Frequency-adaptive pole placement for parallelized proportional, integral and resonant control systems. In *IECON 2025 – 51st Annual Conference of the IEEE Industrial Electronics Society*, pages 1–7. IEEE.

[171] Christoph Göttsberger, Dietmar Fehrenbach, Marek Galek, and Christoph M. Hackl. A generic observer-based control system for three-phase parallel active power filters. In *IECON 2025 – 51st Annual Conference of the IEEE Industrial Electronics Society*, pages 1–8. IEEE.